Pilz, M., Cotton, F., Zaccarelli, R., Bindi, D. (2019): Capturing Regional Variations of Hard-Rock Attenuation in Europe. - *Bulletin of the Seismological Society of America*, *109*, 4, pp. 1401—1418.

DOI: http://doi.org/10.1785/0120190023

Capturing regional variations of hard-rock attenuation in Europe

Marco Pilz[1], Fabrice Cotton[1,2], Riccardo Zaccarelli[1], Dino Bindi[1]

1 Helmholtz Centre Potsdam – German Research Centre for Geosciences GFZ, Telegrafenberg, 14467 Potsdam, Germany

2 Universität Potsdam, Institut für Erd- und Umweltwissenschaften, Karl-Liebknecht-Str. 24-25, 14476 Potsdam, Germany

Corresponding author:

Marco Pilz
Helmholtz Centre Potsdam – German Research Centre for Geosciences GFZ
Seismic Hazard and Risk Dynamics
Telegrafenberg
14467 Potsdam
Germany
Phone: +49 331 288 28661
Email: pilz@gfz-potsdam.de

Abstract

A proper assessment of seismic reference site conditions has important applications as they represent the basis on which ground motions and amplifications are generally computed. Besides accounting for the average S wave velocity over the uppermost 30 m (v_S^{30}), the parameterization of high-frequency ground motions beyond source-corner frequency has received significant attention. κ, an empirical parameter introduced by Anderson and Hough (1984), is often used to represent the spectral decay of the acceleration spectrum at high frequencies. The lack of hard-rock records and the poor understanding of the physics of κ introduced significant epistemic uncertainty in the final seismic hazard of recent projects Thus, determining precise and accurate regional hard-rock κ_0 values is critical. We propose an alternative procedure for capturing the reference κ_0 on regional scales by linking the well-known high-frequency attenuation parameter κ and the properties of multiple-scattered coda waves. Using geological and geophysical data around more than 1300 stations for separating reference and soft soil sites and based on more than 10,000 crustal earthquake recordings, we observe that κ_0 from multiple-scattered coda waves seems to be independent of the soil type but correlated with the hard-rock κ_0, showing significant regional variations across Europe. The values range between 0.004 s for northern Europe and 0.020 s for the southern and south-eastern parts. On the other hand, measuring κ (and correspondingly κ_0) on the S wave window (as classically proposed), the results are strongly affected by transmitted (reflected, refracted and scattered) waves included in the analysed window biasing the proper assessment of κ_0. This effect is more pronounced for soft soil sites. In this way, κ_0^{coda} can serve as a proxy for the regional hard-rock κ_0 at the reference sites.

Introduction

The definition of a standard reference site is a key issue for any seismic hazard analysis since it is highly beneficial when ground motion prediction equations (GMPEs) are referenced to a specific site condition. Reference site properties can vary significantly from one region to another, and recent projects on probabilistic seismic hazard assessment (for example Seismic Hazard Harmonization in Europe, Woessner et al., 2013) and ground motion attenuation relationships (e.g., NGA-East) have shown the need to clearly define reference hard-rock conditions for seismic hazard computations (e.g., Scherbaum et al., 2004, Delavaud et al., 2012, Hashash et al., 2014). Definitions of reference site conditions, however, are highly heterogeneous, mainly due to the high material variability in the shallower layers, and have evolved over the last few years. The S wave velocity v_S, the most commonly used parameter, is usually only measured down to shallow depths and 30 m is often used as the reference depth to which the travel time based average S wave velocity is calculated (v_S^{30}). v_S^{30} alone, however, is considered to be insufficient for the definition of a reference site as it does not capture the effects of shallow crustal attenuation (e.g., Harmsen, 1997, Mucciarelli and Gallipoli, 2006, Lee and Trifunac, 2010, Chiara et al., 2018). The local site conditions can control a significant part of the high-frequency attenuation (Silva et al., 1998, Chandler et al., 2006, Edwards et al., 2011, Kishida et al., 2014). While this high-frequency decay was initially modelled by Hanks (1982) through a frequency value above which the spectrum declines, Anderson and Hough (1984) empirically introduced an exponential decay model

$$A(f) = A_0 e^{-\pi\kappa(r)f} \text{ with } f > f_1. \quad (1)$$

in which A_0 is a source- and propagation-path-dependent amplitude, f_1 is the frequency above which the decay is approximately linear, r is the epicentral distance, and κ is an empirical spectral decay factor κ. The dependence on distance can be eliminated by linearly extrapolating the trend of $\kappa(r)$ to $r = 0$, introducing a site-specific κ, typically denoted as κ_0, that is free of the regional attenuation effect added by distance.

As the number of hard-rock sites is generally limited, the usual practice is to infer the target κ_0 from existing correlations between v_S^{30} and κ_0. There is, however, a large scatter in existing correlations, meaning that these approximations are very poorly constrained. Additionally, the measurement procedure and the studied region may increase the level of uncertainty in such correlations (e.g., Silva et al., 1998, Chandler et al., 2006, Van Houtte et al., 2011, Ktenidou et al., 2014, Edwards et al., 2015).

Ktenidou et al. (2015) recently noted that κ_0 is not only influenced by the very shallow layers beneath the site but it contains the upper local site effect (κ_{top}) caused by the entire soil column beneath the receiver. As κ_0 was found to stabilize for high values of v_S^{30} (Ktenidou et al., 2015), κ_0 can be written as a combination of κ_{top} and a κ_{0ref} related to the regional (reference) attenuation effect,

$$\kappa_0 = \kappa_{\text{top}} + \kappa_{0\text{ref}}. \tag{2}$$

The existence and proper assessment of a regional reference κ_{0ref} have strong implications for high-frequency ground motions (Boore et al., 2003), site-specific hazard assessment (e.g., Budnitz et al., 1997, Rodriguez-Marek et al., 2014) and adjustment of GMPEs for specific sites (e.g., Cotton et al., 2006, Laurendeau et al., 2013, Al Atik and Youngs, 2014). Due to a limited number of reference hard-rock stations it might yet be difficult to separate the two distinct contributions of κ_{top} and κ_{0ref}

for many sites. Moreover, numerical simulations by Parolai et al. (2015) and Parolai (2018) confirmed that a direct estimate of κ^{AH} (and correspondingly also κ_0^{AH}) on the S wave window (as classically done, Anderson and Hough, 1984) is strongly affected by the existence of transmitted (reflected, refracted and scattered) waves in the analysed window leading to strongly biased attenuation (overestimated κ_0^{AH} and underestimated Q_S) estimates. While borehole measurements could help in properly assessing hard-rock values, they go along with high costs.

To overcome this shortcoming, Mayor et al. (2018a) suggested that multiple-scattered coda waves can be used for determining κ_{0ref}. This new approach was motivated by the fact that coda waves decays are insensitive to source and local site effects (e.g. Rautian and Khalturin, 1978, Sato and Fehler, 1998) and have been shown to reflect regional variations of the attenuation (Akinci and Eyidogan, 2000, Guo et al., 2009, De Lorenzo et al., 2013, Kumar et al., 2016). In particular, at long lapse times, coda waves are composed of multiply scattered waves and enter the diffusive regime. For simple models containing a heterogeneous layer overlying a half-space, Q_{coda} asymptotically approaches the intrinsic Q_i of the underlying uniform half-space (Shapiro et al. 2000). These results are consistent with Calvet et al. (2013) who observed that at frequencies higher than a few Hz, the Q_{coda} pattern cannot be related anymore to the shallow layers. As the frequency increases, energy transport by body waves becomes more and more efficient and enhances the sensitivity of the coda to deeper crustal structures (Aki and Chouet 1975). Recently, Mayor et al. (2018a) confirmed that κ_0^{coda} (the high frequency decay of coda waves) does not vary with soil type but shows significant regional variations. They further suggested a correlation between κ_0^{AH} measured at rock sites and κ_0^{coda}. This study, however, suffered from the scarcity data used and Mayor et al. (2018a) concluded that further studies were needed to statistically validate the robustness of the relation between the regional κ_0^{coda} and κ_0^{AH} .

The goal of study is then to test the working hypothesis of Mayor et al. (2018a) and more generally capture and discuss the regional variations of hard-rock attenuation across Europe using geological and geophysical data of more than 1300 stations and 10,000 crustal earthquake recordings. After describing an automatic method for defining the seismic phases and for determining κ_0^{coda} on a large pan-European data set, we will show that the values of κ_0^{coda} are independent of the local site conditions while they strongly regional-depend. We will discuss the reliability of the mapped regional κ_0^{coda} measurements and compare the results with κ_0^{AH} measured at reference (hard-rock) sites and soft soil sites which can provide information about the amount of scattering in the uppermost crust.

Seismic phase windowing

In the literature, a number of approaches for measuring κ exist such as broadband inversion techniques and the use of displacement or acceleration spectra (see, for example, Schneider et al., 1993, Silva et al., 1997, Biasi and Smith, 2001 as well as an overview by Ktenidou et al., 2014). Here we follow the classical approach by fitting a linear trend to the high-frequency decay of the acceleration spectrum. As we will determine κ (and correspondingly κ_0) both on the direct S wave spectrum and on the coda spectrum, the S wave and the coda onset times need to be known. The S wave onset T_S is taken as 1 s before the absolute maximum horizontal amplitude. Although being less precise, for the purpose of spectral analysis of the S wave windows, as they are discussed in this paper, such less accurate estimates are acceptable as long as the determined S wave onset time is not later than the arrival time of the main S wave energy.

Following Perron et al. (2017), the S wave duration is defined by a relatively simple scheme taking into account the expansion of the signal due to propagation (approximated by difference of the first arrival times of S and P waves, T_S-T_P) and the influence of the source approximated by the corner frequency f_C while the source term is considered to have only a minor influence for the moderate to large magnitudes used in this study. The duration of the S wave window D_S is then given by

$$D_S = \frac{1}{f_C} + (T_S - T_P). \tag{3}$$

f_C is estimated directly by the Brune (1970) relationship from the seismic moment M_0, considering a large stress drop Δσ of 100 MPa and a mean S wave velocity for the crust of 3500 m/s,

$$f_C = 0.37 v_s \left[\frac{16\, \Delta\sigma\, 10^5}{7 M_0}\right]^{1/3}. \tag{4}$$

Since a very precise estimate of f_C is not critical for the current study, the choice of the rather large stress drop is only due to the fact to avoid any influence of f_C on the corresponding high-frequency spectra. Lower stress drops will cause even lower f_C. Following Kanamori (1977), M_0 is determined from the event's magnitude (the magnitude scale is not critical for the target of this study).

For the coda onset, we follow the definition of Aki (1969) who proposed the beginning of the coda phase as twice the S wave travel time after the occurrence of the earthquake. To be independent of the available information extracted from the seismic bulletins, Perron et al. (2017) proposed an equivalent formulation based only on T_P and T_S parameters only, i.e.

$$T_{\text{coda}} = 2.3(T_S - T_P) + T_S. \tag{5}$$

This definition of T_{coda} has the advantage of being independent of the uncertainty of the earthquake's origin time. Perron et al. (2017) have found that Equation (5) is able to identify precisely the beginning of the coda phase for local events which are only encountered in this study. The multiple-scattering model requires the attenuation of coda waves to be measured from a time window at sufficiently long lapse times, typically larger than twice the time it takes for an S wave to go from the source to the receiver (Calvet and Margerin, 2013). Assuming $v_P \geq \sqrt{3}v_S$, T_{coda} from Equation (5) will always be equal or larger than $2T_S$. Finally, the end of the coda phase T_{end} is defined once a threshold of 95% of the cumulative energy is exceeded (Trifunac and Brady, 1975). An example of phase intervals and nomenclature is given in Figure 1.

The noise window is taken before the P wave arrival T_P with a variable length but only up until 0.5 s before T_P. If a late trigger causes the record to be shorter than this value, the data are discarded. All windows are tapered with a 5%-cosine taper, converted to acceleration through differentiation (if necessary) and transformed to the Fourier domain. Their spectral amplitudes are smoothed using a Konno-Ohmachi filter (Konno and Ohmachi, 1998) with a bandwidth $b = 40$.

For the calculation of κ, we fit a straight line in a variable frequency range $[f_1, f_2]$ to the S wave and coda acceleration spectra. f_1 should lie well above the source corner frequency and f_2 should lie below the frequency at which the noise floor begins. In the suggested algorithm, a range of frequencies for both f_1 (f_C + 2 Hz to 18 Hz with a Δf_1 of 1 Hz) and f_2 (f_1 + 10 Hz to 40 Hz with a Δf_2 of 3 Hz) is used. For the automatic approach, we use only events with $M > 3.5$ and set the minimum value of f_1 at 10 Hz noting that $f_C = 10$ Hz is equivalent to a stress drop of approximately 100 MPa at $M_w = 3.5$ (with lower stress drops and/or larger magnitudes leading to lower f_c).

The RMS residual E between the smoothed spectrum and the fit is calculated for each frequency band Δf between f_1 and f_2, and followed by a division by the square-root of the respective bandwidth,

$$P = \frac{E}{\sqrt{\Delta f}}\,. \quad (6)$$

The parameter *P* depicts a quantitative criterion for fitting a straight line over a variable frequency range adjusted by its width used to obtain this measure. The motivation for picking a rather straight line (and a corresponding small RMS residual) over a broad spectral range (large Δf) is assigned by choosing the lowest *P* value for the actual measurement of κ. Strong deviations due to spectral curves or bulges are considered being less acceptable by this algorithm, as the corresponding values of *E* would be significantly higher than those from a more linear section. In this way, the influence of site resonance peaks, which can cause significant variability in κ (Parolai and Bindi 2004, Kishida et al., 2014, Van Houtte et al., 2014, Edwards et al., 2015, Laurendeau et al., 2017), is minimized. Additionally, deviations from a straight line due converging to the noise level in the high-frequency range or further irregularities are mostly excluded as long as a sufficiently linear spectral range exists in the main part of the spectral window fulfilling the signal-to-noise (SNR) criterion.

The harmonic mean of the spectral ratio of the signal to the pre-event noise at all frequencies is used for calculating the SNR. This criterion is less strict than limiting the bandwidth to a single frequency value for which the SNR will fall below a certain threshold, as this might occur already at much lower frequencies if the spectra contains narrow spikes or troughs, whereas on average the SNR might still be considered acceptable. On the other hand, the arithmetic average is generally too insensitive to low values while the harmonic mean might strongly decrease in the presence of a few low values which might result in a too conservative average. For our study, the SNR limit is set to 4, in turn excluding frequency bands falling below this threshold for further analysis. In the end, the best estimate for κ (dotted line in Figure 2) minimizing the RMS is taken with its associated uncertainty.

Once the individual κ values are computed for each site for the S wave and for the coda windows, we follow the classical approach (Anderson and Hough, 1984) and perform an automatic linear regression with epicentral distance but only if the distance range was larger than 25 km. We remark that, as acknowledged by Hough et al. (1988), there is no reason to expect a linear dependence for small distance ranges, although they say that it is a reasonable first order approximation (see also Boore and Campbell, 2017). Since only for very few sites we observed a flattening of κ with distance for distances less than 50 to 60 km without any regional pattern (not shown), the κ value at the intercept of the straight line with the minimized epicentral distance $r = 0$ is taken as κ_0.

Data set

The main database is composed of seismic events that were recorded between January 2000 and December 2017. All data have been downloaded from the EIDA (European Integrated Data Archive) data centres and processed using the stream2segment software (Zaccarelli et al., 2019). EIDA currently offers uniform data access via standard FDSN (Federation of Digital Seismograph Networks) protocols to unrestricted data from 10 European nodes, hosting data from about 100 permanent and a large number of temporary networks.

Only events with $M > 3.5$ have been used, ensuring a sufficiently high SNR over a broad frequency range. We rejected events coming from subduction regimes, thus limiting the focal depths to a maximum of 30 km. For ensuring that the propagation is only in the crust, only events with epicentral distances less than 120 km have been used. For each station, we require at least five recordings. Starting from more than 4000 stations available, we created a subset of more than 87,000 recordings (velocity and acceleration seismograms) of 10,732 events at 1384 sites. Their geographical distribution and a magnitude-distance representation are shown in Figure 3.

Lapse-time dependence and window length sensitivity

For the S wave window and the corresponding κ_0^{AH}, several studies have already investigated the influence to the duration of the signal window (e.g., Tsai and Chen, 2000, Douglas et al., 2010). These studies have mostly concluded that there is only a limited dependence of the window length on the determination of κ_0^{AH}, as long as the most energetic part is encapsulated in the selected time window. For the determination of κ_0^{coda}, however, a proper choice of the coda window is crucial. In particular, if different coda phases are mixed during the analysis (i.e. early and late coda phases), it might be difficult to separate variations of the epicentral distance from spatial variations of κ^{coda} and correspondingly κ_0^{coda} (Calvet and Margerin, 2013, Mayor et al., 2016).

For avoiding biased κ_0^{coda}, the epicentral distance range must be bounded, and the coda window parameters (onset and duration) must be chosen in a way such that the measurements are free from any lapse-time dependence. To convince the reader of the robustness of the applied criterion, we show in Figure 4 κ_0^{coda} for different choices of the coda window length L_{coda} and different coda onset times T_{coda}. κ_0^{coda} typically ranges between 0.01 and 0.05 for a window length between 5 and 35 s and a fixed onset time of 20 s. This is likely due to events at larger epicentral distances for which the ballistic time of the S waves is close to the coda window onset, meaning that these waves have not entered the multiple-scattering regime. On the other hand, κ_0^{coda} is smaller and largely time-independent for an onset time of $T_{\text{coda}} = 40$ s (Figure 4 middle), meaning that the dependence of κ_0^{coda} on L_{coda} is strongly affected by the value of T_{coda} but shows a larger standard deviation on average. A coda window onset of $T_{\text{coda}} = 2.3(T_S - T_P) + T_S$ (Figure 4 right) and a sufficiently long coda window length of at least 15 s seems to provide the best compromise for stable values of κ_0^{coda} since only stable values of κ_0^{coda} for varying L_{coda} can be considered as an approximation of the intrinsic attenuation (similar to the observations of Calvet and Margerin 2013). This procedure is particularly important when performing a regionalization of κ_0^{coda} over a broad region. In this way, the range of fluctuations for κ_0^{coda} indicates the strong lateral variations of the attenuation across Europe and only partially reflects the measurement uncertainties.

Regional variations of κ_0

Figure 5 presents the regional variations of κ_0^{coda} across Europe interpolated between 1363 sites. We note that for 21 sites (1.6 % of the total number of sites) no reliable values of κ_0^{coda} have been obtained by the automatic procedure (i.e., negative values for 17 sites and unrealistically high values with $\kappa_0^{\text{coda}} \gg 0.1$ s for four sites). If hypothesizing that κ_0^{coda} captures only attenuation, then negative values of κ_0^{coda} are physically not realistic. However, κ_0^{coda} is an empirical parameter, meaning that the measurements might therefore be influenced by further site-specific unmodelled phenomena, such as particular site conditions and anisotropy.

Linearly interpolating between the 1363 remaining sites, we observe a clear regional pattern with strong attenuation ($\kappa_0^{\text{coda}} > 0.014$ s) for the southern and south-eastern part of Europe while central and northern Europe, as far as the station coverage allows to conclude, shows significantly lower attenuation values ($\kappa_0^{coda} \lesssim 0.008$ s). The physical reason for such regional pattern might be due to the fact that coda waves are mainly sensitive to the attribues of the crust within a radius of around 0.25*l* (with *l* being the scattering mean free path which is of the order of 100 km for the standard crust) around the source and the station, when the time in the coda is equal to twice the time of the *S* wave (Mayor et al. 2014). Regarding our epicentral distance range (less than 120 km) and the position of the coda window, we can infer that coda waves tend to average the properties of the crust in the volume between the source and the station. Moreover, we expect that the coda wave trains sample almost the same volume of the crust around each station in each region of investigation but we cannot exclude that attenuation may be depth-dependent due to changes in material properties.

Influence of soil properties

Since previous studies have indicated that the local soil properties can have a significant impact on κ_0^{AH}, we try to identify the effects of the shallow soil characteristics on κ_0^{coda}. To this regard, we try to differentiate our results between sites which might serve as regional reference (hard-rock) sites and sites characterized by significant local amplification effects. To do so, in a first step, each network site has been assigned to a lithology class following the harmonized pan-European surface geological map (European Geological Data Infrastructure EGDI, 2017). Herein, lithological descriptions follow the official INSPIRE (INfrastructure for SPatial Information in EuRopE) reference document (INSPIRE, 2013). Variations of rock and stone types are identified as reference sites whereas sand, clay and sedimentary materials are identified as non-reference sites.

As only earthquake recordings are available in a consistent manner for all instrumented sites, in a second step, we classify the network sites according to their horizontal-to-vertical (H/V) spectral ratio from earthquake recordings (Lermo and Chavez-Garcia, 1993). At each site, each S wave window D_S was cosine-tapered (5 per cent) and a Fast Fourier Transformation (FFT) for each seismometer component was performed. Spectral amplitudes were smoothed using the Konno and Ohmachi (1998) recording window (b = 20). Finally, the horizontal spectrum was calculated considering the root-mean square average of the two horizontal component spectra and divided by the vertical spectrum.

In seismic site response analysis, a reference site is generally defined as a site without significant resonances. Resonances, however, can also develop due to energy trapped in shallow low-velocity layers even at sites with high values of v_S^{30} (Boore, 2004, Cadet and Duval, 2009). Since reference sites can be considered not being absolutely free from amplification effects due to their S wave velocity gradient, we require the H/V spectral ratio for reference sites to be sufficiently flat in a frequency range between 0.2 and 10 Hz with an amplitude less than 2.5, hereby slightly relaxing the proposal of Zhao et al. (2006). H/V spectral ratios of reference sites are shown in Figure 6.

In total, out of 1363 sites for which κ_0^{coda} has been calculated, only 717 sites fulfil both the criterion on geology and on H/V. These sites are classified as reference sites in the following and listed in Appendix A1. 456 sites were identified as non-reference sites while for 190 sites no clear classification could be made.

We try to identify differences between reference and non-reference sites due to shallow soil layers on κ_0. Figure 7 plots κ_0^{AH} and κ_0^{coda} for the both site classes. While κ_0^{coda} seems to be independent of the soil type (as can be seen in Figure 5), clear differences between reference and non-reference sites can be observed for κ_0^{AH}. For non-reference sites, on average, higher values for κ_0^{AH} are observed with respect to κ_0^{coda} while there is only a limited number of non-reference sites for which κ_0^{coda} is larger than κ_0^{AH}.

Reliability of the proposed κ_0^{coda}

As measurements of κ and κ_0 generally go along with large scatter, a number of quantitative quality criteria have been developed including standard deviations from each slope (Lai et al., 2016) as well as from the combination of the two horizontal components' κ (Purvance and Anderson, 2003), using several spectral windows to obtain a mean and standard deviation (Ktenidou et al., 2016) and using the fitted slope's standard error or the variability from different component orientations (Van Houtte et al., 2014).

In a first step, we rely on the parameter *P*, as defined by Equation (6), quantifying the quality of the spectral fit. Averaged over all recordings and all 1363 sites, *P*, and correspondingly Δκ, indicates a decay proportional with $\sqrt{\Delta f}$ (not shown). Although the sensitivity of Δκ to Δf is mainly linked to source and site effects, in our case, site resonance peaks can be considered having only a minor influence on the variability of κ (see description of the methodology above). Moreover, for multiple-scattered coda waves, the source effects are also averaged out assuming the validity of the Brune (1970) source model. Simple models varying other source parameters (such as the take-off angle) highlight that the apparent decay of displacement will not always be ω^2 (e.g., Madariaga, 1976) but this uncertainty of Δκ decreases significantly as magnitude increases (Perron et al., 2017) and can therefore be considered to be of minor influence. Since we apply an automatic method for phase picking phases, we avoid additional uncertainty to the κ calculations due to a manual picking of phases (Douglas et al 2010).

To verify the magnitude independence of κ_0^{coda}, we also present κ_0^{coda} as a function of magnitude (Figure 8). As stated above, the magnitude scale has been assumed to be not critical for the target of this study. We calculate κ_0^{coda} separately for magnitude bins with a width of 0.5 magnitude units.

Since only events with $M > 3.5$ have been used, meaning that we can exclude any influence of f_C, there is no significant dependence on magnitude for κ_0^{coda}. Such results is consistent with previous findings of, e.g., Fernández et al. (2010), Van Houtte et al. (2014) and Castro and Ávila-Barrientos (2015) who also observed no or little correlation of κ_0 with magnitude.

For a quantitative and objective approach to quantify the randomness and the degree to which similar κ_0^{coda} features cluster, we calculate the spatial autocorrelation based on Moran's I test (Moran 1948). While positive values for I indicates that neighbouring features with similarly high or properties exist (i.e., this feature is part of a cluster), a negative value for I indicates that a feature has neighbouring features with dissimilar values (i.e., this feature can be considered an outlier). Values close to zero indicate a random pattern. Using distances of 50 and 100 km, no negative values for I are observed but the global Moran's I index takes values of 0.58 and 0.42 ($p < 0.05$), which indicates a strong and positive spatial correlation.

Furthermore, we calculate the standard error of the mean and the standard deviation of the data points. The former, representing the confidence intervals around the estimated mean values of κ_0, generally takes values around 0.002 to 0.003 s for κ_0^{coda} and κ_0^{AH}. Although this does not fully reflect the standard deviations of the measured κ_0 values, it can still provide high confidence in the mean κ_0^{coda} and κ_0^{AH} values. The standard deviation, on the contrary, is rather high, taking values of $\Delta\kappa_0^{\mathrm{coda}} = 0.0068$ s and $\Delta\kappa_0^{\mathrm{AH}} = 0.0082$ s. Because rock sites tend to be more variable (Schneider et al., 1993), we also calculate $\Delta\kappa_0$ separately for reference and non-reference sites. While the former show an $\Delta\kappa_0^{\mathrm{coda}} = 0.0078$ s and $\Delta\kappa_0^{\mathrm{AH}} = 0.0092$ s, soft sites are characterized by less variability as $\Delta\kappa_0^{\mathrm{coda}} = 0.0055$ s and $\Delta\kappa_0^{\mathrm{AH}} = 0.0063$ s. Since we consider the wide distribution of distances, we do not observe better constrained values κ_0 values restricting the analysis to smaller distance ranges.

Although the low values of the error of the mean might imply that we need a large number of records to get a reliable estimate of the mean κ_0 value, Kendall's τ correlation coefficient between the number of records at a single station and $\Delta\kappa_0$, which measures the ordinal association between the two variables taking values between +1 and -1 (with +1 representing a total positive correlation and 0 representing no linear correlation), takes values of only 0.17 for the S wave portion and 0.21 for the coda window. This indicates that there is only a slight correlation between the number of records and the uncertainty in κ_0^{coda} and κ_0^{AH} as long as a sufficient number of high-quality records is available.

In this way, since κ_0^{coda} seems not to be affected by the shallow surface layers (κ_{top} in Equation 2), it might serve as a lower bound estimate for the regional hard-rock reference κ_0^{AH} ($\kappa_{0\mathrm{ref}}$ in Equation 2). The existence of such a reference κ_0^{AH} has already been suggested by Ktenidou et al. (2015) and Mayor et al. (2018a) have argued that κ_0^{coda} can be seen as the weighted time (weighted by attenuation properties quantified by coda) spent by the wave in the crust. In practice, when site-specific data is not available (for instance, when adjusting a GMPE to a stable continental region with little seismic activity and instrumentation), κ_0 is often inferred from available site data, mainly v_S^{30} along with large scatter and limited applicability (e.g., Ktenidou et al., 2011, 2014, Van Houtte et al., 2011, Biro and Renault, 2012).

For this reason, we now revisit if the regional κ_0^{coda} can serve as a proxy for the regional κ_0^{AH} at reference sites. To this regard, we compare the interpolated κ_0^{coda} from Figure 5 and the measured S wave κ_0^{AH} at reference sites (Figure 9). A clear and positive correlation between measured κ_0^{AH} and interpolated κ_0^{coda} is found. In general, the patterns of these two data sets seem to exhibit considerable mutual similarity and similar trends. For the two variables, the Pearson correlation coefficient, being based on the assumption that we have bi-variable normal distributions and similarly taking values between +1 and -1 (with +1 representing a total positive linear correlation), is equal to 0.71. Such value is significantly higher than previously found correlations coefficients in most κ_0-v_S^{30} correlations with values ranging between less than 0.3 (Ktenidou et al., 2014) and 0.4 (Van Houtte et al., 2011). Of course, besides large uncertainties in properly assessing κ_0, there is also a significant uncertainty in the estimation of v_S^{30}. In turn, while many studies conclude that v_S^{30} as a proxy for assessing κ_0 cannot lead to accurate estimations of the attenuation and its variability (e.g., Laurendeau et al., 2013, Cabas et al., 2017), inferring κ_0 from existing κ_0^{coda} maps might allow better constraining the regional dependence of attenuation (in agreement with the findings of Ktenidou et al., 2014).

Comparison of attenuation models

Until a regionalized site-response model for the calculation of surface ground motion is developed, hypothetical velocity reference profiles (e.g., Petersen et al., 2008, Poggi et al., 2011, Woessner et al., 2013) remain the only possibility for estimating ground motions. It might, however, be difficult to properly mimic its attenuation properties and to properly constrain the profile's κ_0 given that κ_0 can often not be directly estimated from local waveform data. Therefore, one way of choosing an appropriate attenuation value is fixing κ_0 based on its correlation to v_S^{30} but such correlations are very weak and many possibilities exist for κ_0 for different sites with the same v_S^{30}.

Another possibility for fixing κ_0 is to compare the amplification factors predicted from given velocity profiles and varying the candidate values of κ_0 with site coefficients used in the building codes (e.g., Campbell, 2009). However, our map in Figure 5 can provide direct lower bound estimates for the regional reference κ_0. The measured κ_0^{coda} are rather free from soil-type and source effects and mimic the regional attenuation variations.

Although only a limited number of studies have published regional variations of κ_0^{coda}, our results are relatively consistent with literature: Mayor et al. (2018a) identify clear differences between northern and south-eastern France with low attenuation (low values of κ_0^{coda}) for the central southern part. The sedimentary southeast basins in the extreme south-eastern part of France, on the contrary, are characterized by higher attenuation values with $\kappa_0^{coda} > 0.01$ s.

While the use of κ_0^{coda} is currently limited, further studies have focused on calculating localized κ_0^{AH} values for various site conditions across Europe. For Switzerland, the values obtained in the present study are reasonably consistent with the 0.0125 s value for hard-rock stations obtained by Bay et al. (2005) and the 0.012 s value for the western Alps found by Morasca et al. (2006) although they were using a different technique. Douglas et al. (2010) and by Drouet et al. (2010) indicate values of κ_0^{AH} in the order of 0.008 to 0.03 s for France and the Pyrenees with some variations between the two studies due to differences in data processing (site effect corrections, frequency range). García-García et al. (2002) examined stations near the Granada basin and found κ_0^{AH} between 0.006 to 0.04 s depending on the local soil conditions, confirming the results shown in Figure 7. For Croatia, Stanko et al. (2017) indicated κ_0^{AH} ranging from 0.016 s for stations in the southern part of the country to 0.027 s for northern sites. While there is a clear correlation between κ_0^{coda} values in Figure 5 and the classical κ_0^{AH} analysis for hard-rock and reference sites, the κ_0^{AH} values in studies focusing only on soft and very soft sites (e.g., Dimitriu et al., 2001, Askan et al., 2014) are significantly larger, in agreement with the results presented in Figure 7. It seems rather obvious that such differences might be caused mainly by attenuation effects of the soft surface materials.

In general, attenuation can be caused by scattering as well as anelasticity and several studies have already shown that κ_0^{AH} results both from anelasticity and scattering: Ktenidou et al. (2015) compared their estimates of κ_0^{AH} with the values of Q_S for the Euroseistest area and concluded that their κ_0^{AH} observations cannot be explained by intrinsic Q_S values alone, meaning that there is a high probability of an additional scattering contribution in their S wave window. Rodriguez-Marek et al. (2017) have shown that neglecting scattering are liable in practice to fail for high-frequency waves. Also in our study scattering due to superficial soil layers at non-reference sites seems to strongly influence the values of κ_0^{AH} (Figure 7, see also Parolai et al., 2015, Pilz and Fäh, 2017, Parolai, 2018), therefore hiding any regional pattern for κ_0^{AH}. While scattering and intrinsic attenuation are difficult to separate in a classical κ_0^{AH} analysis (even on rock), this separation may be easier using κ_0^{coda} and varying the coda window length. Indeed, our analysis of κ_0^{coda} over short and long windows (Figure 4) shows, on average, an increase in κ_0^{coda} when using the shorter early coda windows. Compared to soft sites, this effect is less significant but not negligible at reference sites. This suggests that κ_0^{coda} may be controlled both by scattering and anisotropy effects when measured close to the S wave phase. At large lapse time in the coda, however, coda waves can be seen as multiple-scattered waves having entered the diffusive regime and the mapped κ_0^{coda} represents the intrinsic κ_0.

In this way, the results of Figure 7 further confirm the findings of Jin et al. (1994, their Figure 9) who compiled studies from several regions around the world and concluded that Q_{coda} is close to Q_S only when the scattering contribution is small. Strong deviations are found for measurements at frequencies smaller than 6 Hz (Mayeda et al., 1992). Therefore and following Calvet and Margerin (2013), Q_{coda} for large lapse times (multiple-scattering regime) alone can be seen as an approximation of the intrinsic quality factor which quantifies the average attenuation properties of the crust.

It is obvious that the effect of scattering is expected to be frequency-dependent as different wavelengths will interact in different ways with the velocity discontinuities (generally indicated through the definition of different scattering regimes) that they encounter during propagation. In turn, when a segment of the S wave signal is considered, as generally done in standard κ_0^{AH} assessments, the values might differ greatly and may strongly be dependent on the chosen frequency band and not accounting for the influence of scattering on κ_0^{AH} may be problematic for high frequencies (Richards and Menke, 1983), mainly due the complicated shape of the identified S wave pulse.

While previous studies (e.g., Edwards et al., 2015, Mayor et al., 2018a) relied on a fixed frequency band for the automatic calculation of κ_0^{AH}, we allowed some variability for the frequency range for aiming at the best linear fit (lowest RMS) over a broad spectral range (at least 10 Hz) for κ_0^{AH} and κ_0^{coda}. Trials using a fixed frequency band were carried out as well but most of such cases turned out to be bad choices since disturbing effects such as site resonance peaks have been included. A human analyst would identify such situations and disregard the chosen frequency range but such approaches are hardly feasible for large data sets. Although the automatic procedure will not be free from biased κ estimates, in the absence of alternative models, the approach adopted here tries to minimize, at first order, epistemic uncertainty in κ_0^{coda} measurements.

We should keep in mind that the concept of κ, moreover being frequency-independent, is a rather simple empirical model for an observation without providing a full explanation of the physical basis. Any frequency-dependent inelasticity due to spectral variations of the scatters density is certainly possible and likely to be present in Earth's crust. In this way, accounting for the frequency-dependence of κ_0^{AH} could provide some constraints on the roughness and the scattering properties of the shallow layers.

Conclusions

A first attempt of mapping regional variations of κ_0^{coda} attenuation across Europe has been proposed based on the analysis of local crustal earthquakes. Using more than 10,000 moderate to large magnitude events that have occurred in Europe after January 2000, for each record, we performed two sets of κ measurements on the S wave portion and on the late coda window over a broad but variable spectral band. For the automatic selection of the earthquake signal phases, our analysis is based on P and S wave arrival times only, making the windowing independent of uncertainties of the seismic bulletins.

We observed that κ_0^{coda} for large lapse times does not vary with soil type but shows significant regional variations. The map indicates distinct regional attenuation patterns with stronger attenuation for the southern and south-eastern parts of Europe while much lower attenuation values are found for the northern parts. This analysis confirms previous findings of Mayor et al. (2018a, 2018b) who showed that κ_0^{coda} can be used as a proxy to capture the regional reference κ_0 and the corresponding intrinsic attenuation if κ_0^{coda} is measured on the latest part of the coda. Current GMPEs are not able to take into account these regional variations thereby introducing large uncertainties in ground motion estimates. To overcome this limitation, next generation GMPEs should obviously incorporate spatial variations in the decay of the shallow seismic attenuation properties. The task of constructing region-dependent GMPEs might be facilitated by high-resolution attenuation maps such as the one produced in this work.

Comparing the large lapse-time κ_0^{coda} and κ_0^{AH} (classically determined on the S wave window), we see that the latter is strongly affected by transmitted waves included in the analysed window, further indicating a clear dependence on the local soil properties which might be indicative of stronger (and frequency-dependent) scattering properties of the shallow soft layers. In this way, because the classical κ_0^{AH} might not be able to correctly capture the absolute intrinsic attenuation, in combination with κ_0^{coda} measured on various time windows, it might provide some indication about the amount of scattering in the uppermost crust and surface layers.

For mapping regional variations of κ_0^{coda}, we fully relied on classical methodologies and properties of multiple-scattered coda waves which have widely been applied in seismological studies. Future works might further quantify the effects of intrinsic and scattering attenuation κ_0^{AH} and explore the sensitivity of κ_0^{coda} measurements to depth variations of absorption. It is clear that our simple mapping approach can only provide the gross features of the lateral variations of attenuation without any constraint on the depth behaviour.

Data and resources

The European Integrated Data Archive (EIDA, www.orfeus-eu.org/eida, last accessed January 2019) strong ground motion database was searched for this publication.

Acknowledgments

The authors would like to thank the different organisms who operate seismological networks across Europe and for making their data available through EIDA. We are thankful to associate editor Sheri Molnar, Gail Atkinson and one anonymous reviewer for the useful comments and suggestions. We warmly Marie Calvet, Jessie Mayor and Ludovic Margerin for their stimulating discussions and explanations about the coda. This study has been partially funded by the H2020 project SERA (Seismology and Earthquake Engineering Research Infrastructure Alliance for Europe, grant agreement No. 730900).

References

Aki, K. (1969). Analysis of the seismic coda of local earthquakes as scattered waves. *Journal of Geophysical Research*, **74**, 615-631.

Aki, K. (1980). Quantitative seismology. Theory and Methods, New York, W. H. Freeman and Co.

Aki, K., Chouet, B. (1975). Origin of coda waves: source, attenuation, and scattering effects. *Journal of Geophysical Research*, **80**, 3322-3342.

Akinci, A., Eyidoğan, H. (2000). Scattering and anelastic attenuation of seismic energy in the vicinity of north Anatolian fault zone, eastern Turkey. *Physics of the Earth and Planetary Interiors*, **122**, 229-239.

Al Atik, L., Youngs, R. R. (2014). Epistemic uncertainty for NGA-West2 models. *Earthquake Spectra*, **30**, 1301-1318.

Anderson, J. G., Hough, S. E. (1984). A model for the shape of the Fourier amplitude spectrum of acceleration at high frequencies. *Bulletin of the Seismological Society of America*, **74**, 1969-1993.

Askan, A., Sisman, F. N., Pekcan, O. (2014). A regional near-surface high frequency spectral attenuation (kappa) model for northwestern Turkey. *Soil Dynamics and Earthquake Engineering*, **65**, 113-125.

Bay, F., Wiemer, S., Fäh, D., Giardini, D. (2005). Predictive ground motion scaling in Switzerland: best estimates and uncertainties. *Journal of Seismology*, **9**, 223-240.

Biasi, G. P., Smith, K. D. (2001). Site effects for seismic monitoring stations in the vicinity of Yucca Mountain, Nevada. MOL20011204, 0045. Report for the US DOE/University and Community College System of Nevada (UCCSN) Cooperative Agreement.

Biro, Y., Renault, P. (2012). Importance and impact of host-to-target conversions for ground motion prediction equations in PSHA. *Proceedings of the 15th World Conference on Earthquake Engineering*, paper 1855, Lisbon, Portugal.

Boore, D. M. (2003). Simulation of ground motion using the stochastic method. *Pure and Applied Geophysics*, **160**, 635-676.

Boore, D. M. (2004). Estimating Vs30 (or NEHRP site classes) from shallow velocity models (depths< 30 m). *Bulletin of the Seismological Society of America*, **94**, 591-597.

Brune, J. N. (1970). Tectonic stress and the spectra of seismic shear waves from earthquakes. *Journal of Geophysical Research*, **75**, 4997-5009.

Budnitz, R. J., Apostolakis, G., Boore, D. M. (1997). Recommendations for probabilistic seismic hazard analysis: guidance on uncertainty and use of experts (No. NUREG/CR-6372-Vol. 1; UCRL-ID-122160). Nuclear Regulatory Commission, Washington, United States.

Cabas, A., Rodriguez-Marek, A., Bonilla, L. F. (2017). Estimation of site-specific Kappa (κ0)-consistent damping values at KiK-net sites to assess the discrepancy between laboratory-based damping models and observed attenuation (of seismic waves) in the field. *Bulletin of the Seismological Society of America*, **107**, 2258-2271.

Cadet, H., Duval, A. M. (2009). A shear wave velocity study based on the KiK-net borehole data: A short note. *Seismological Research Letters*, **80**, 440-445.

Calvet, M., Margerin, L. (2013). Lapse-time dependence of coda Q: Anisotropic multiple-scattering models and application to the Pyrenees. *Bulletin of the Seismological Society of America*, **103**, 1993-2010.

Campbell, K. W. (2009). Estimates of shear-wave Q and κ0 for unconsolidated and semiconsolidated sediments in Eastern North America. *Bulletin of the Seismological Society of America*, **99**, 2365-2392.

Campillo, M., Plantet, J. L., Bouchon, M. (1985). Frequency-dependent attenuation in the crust beneath central France from Lg waves: data analysis and numerical modeling. *Bulletin of the Seismological Society of America*, **75**, 1395-1411.

Castro, R. R., Ávila-Barrientos, L. (2015). Estimation of the spectral parameter kappa in the region of the Gulf of California, Mexico. *Journal of Seismology*, **19**, 809-829.

Chandler, A. M., Lam, N. T. K., Tsang, H. H. (2006). Near-surface attenuation modelling based on rock shear-wave velocity profile. *Soil Dynamics and Earthquake Engineering*, **26**, 1004-1014.

Chiara, F., Giovanni, L., Rodolfo, P., Lucia, L., Francesca, P. (2018). Ground motion model for reference rock sites in Italy. *Soil Dynamics and Earthquake Engineering*, **110**, 276-283.

Cotton, F., Scherbaum, F., Bommer, J. J., Bungum, H. (2006). Criteria for selecting and adjusting ground-motion models for specific target regions: Application to central Europe and rock sites. *Journal of Seismology*, **10**, 137.

De Lorenzo, S., Del Pezzo, E., Bianco, F. (2013). Qc, Qβ, Qi and Qs attenuation parameters in the Umbria–Marche (Italy) region. *Physics of the Earth and Planetary Interiors*, **218**, 19-30.

Delavaud, E., Cotton, F., Akkar, S., Scherbaum, F., Danciu, L., Beauval, C., Drouet, S., Douglas, j., Basili, R., Abdullah Sandikkaya, M., Segou, M., Faccioli, E., Theodoulidis, N. Segou, M. Toward a ground-motion logic tree for probabilistic seismic hazard assessment in Europe. *Journal of Seismology*, **16**, 451-473.

Dimitriu, P., Theodulidis, N., Hatzidimitriou, P., Anastasiadis, A. (2001). Sediment non-linearity and attenuation of seismic waves: a study of accelerograms from Lefkas, western Greece. *Soil Dynamics and Earthquake Engineering*, **21**, 63-73.

Douglas, J., Gehl, P., Bonilla, L. F., Gélis, C. (2010). A κ model for mainland France. *Pure and Applied Geophysics*, **167**, 1303-1315.

Drouet, S., Cotton, F., Guéguen, P. (2010). Vs30, κ, regional attenuation and Mw from accelerograms: application to magnitude 3–5 French earthquakes. *Geophysical Journal International*, **182**, 880-898.

Edwards, B., Fäh, D., Giardini, D. (2011). Attenuation of seismic shear wave energy in Switzerland. *Geophysical Journal International*, **185**, 967-984.

Edwards, B., Ktenidou, O. J., Cotton, F., Abrahamson, N., Van Houtte, C., Fäh, D. (2015). Epistemic uncertainty and limitations of the κ0 model for near-surface attenuation at hard rock sites. *Geophysical Journal International*, **202**, 1627-1645.

EGDI (2017) 1:1 Million OneGeology pan-european Surface Geology, www.europe-geology.eu (last accessed January 2019).

Fernández, A. I., Castro, R. R., Huerta, C. I. (2010). The spectral decay parameter kappa in northeastern Sonora, Mexico. *Bulletin of the Seismological Society of America*, **100**, 196-206.

Frankel, A., Wennerberg, L. (1987). Energy-flux model of seismic coda: separation of scattering and intrinsic attenuation. *Bulletin of the Seismological Society of America*, **77**, 1223-1251.

García-García, J. M., Romacho, M. D., Jiménez, A. (2002). The corner frequencies, stress drops and apparent stresses of microearthquakes in the Betic region (southern Spain). *Física de la Tierra*, **2002**, 161-182.

Guo, M. Q., Fu, L. Y., Ba, J. (2009). Comparison of stress-associated coda attenuation and intrinsic attenuation from ultrasonic measurements. *Geophysical Journal International*, **178**, 447-456.

Hanks, T. C. (1982). fmax. *Bulletin of the Seismological Society of America*, **72**, 1867-1879.

Harmsen, S. C. (1997). Estimating the diminution of shear-wave amplitude with distance: Application to the Los Angeles, California, urban area. *Bulletin of the Seismological Society of America*, **87**, 888-903.

Hashash, Y. M., Harmon, J., Stewart, J. P., Kottke, A., Kim, B., Silva, W., Rathje, E., Campbell, K. W. (2014). Reference rock site condition for central and eastern North America. *Bulletin of the Seismological Society of America*, **104**, 684-701.

Herrmann, R. B. (1980). Q estimates using the coda of local earthquake. *Bulletin of the Seismological Society of America*, **70**, 447-468.

Hough, S. E., Anderson, J. G., Brune, J., Vernon III, F., Berger, J., Fletcher, J., Haar, L., Hanks, T., Baker, L. (1988). Attenuation near Anza, California. *Bulletin of the Seismological Society of America*, **78**, 672-691.

Houtte, C. V., Ktenidou, O. J., Larkin, T., Holden, C. (2014). Hard-site κ0 (kappa) calculations for Christchurch, New Zealand, and comparison with local ground-motion prediction models. *Bulletin of the Seismological Society of America*, **104**, 1899-1913.

INSPIRE (2013). D2.8.III.3 INSPIRE Data specification on soil – Technical Guidelines, https://inspire.ec.europa.eu/documents/Data_Specifications/INSPIRE_DataSpecification_SO_v3.0rc3.pdf (last accessed January 2019).

Jin, A., Mayeda, K., Adams, D., Aki, K. (1994). Separation of intrinsic and scattering attenuation in southern California using TERRAscope data. *Journal of Geophysical Research*, **99**, 17835-17848.

Kanamori, H. (1977). The energy release in great earthquakes. *Journal of Geophysical Research*, **82**, 2981-2987.

Kishida, T., Kayen, R., Ktenidou, O. J., Silva, W., Darragh, R., Watson-Lamprey, J. (2014). PEER Arizona strong motion database and GMPEs evaluation, Pacific Earthquake Engineering Research Center, PEER Report 2014/09, 170 pages, Berkeley, California.

Konno, K., Ohmachi, T. (1998). Ground-motion characteristics estimated from spectral ratio between horizontal and vertical components of microtremor. *Bulletin of the Seismological Society of America*, **88**, 228-241.

Ktenidou, O. J., Cotton, F., Abrahamson, N. A., Anderson, J. G. (2014). Taxonomy of κ: A review of definitions and estimation approaches targeted to applications. *Seismological Research Letters*, **85**, 135-146.

Ktenidou, O. J., Abrahamson, N. A., Drouet, S., Cotton, F. (2015). Understanding the physics of kappa (κ): Insights from a downhole array. *Geophysical Journal International*, **203**, 678-691.

Ktenidou, O. J., Abrahamson, N., Drouet, S., Cotton, F. (2016). Understanding the physics of kappa (κ0): Insights from the euroseistest network. *Bulletin of the Geological Society of Greece*, **50**, 1515-1524.

Kumar, R., Gupta, S. C., Singh, S. P., Kumar, A. (2016). The attenuation of high-frequency Seismic waves in the Lower Siang Region of Arunachal Himalaya: Qα, Qβ, Qc, Qi, and Qs. *Bulletin of the Seismological Society of America*, **106**, 1407-1422.

Lai T. S., Mittal H., Chao W. A., Wu Y. M. (2016) A study on Kappa value in Taiwan using borehole and surface seismic array. *Bulletin of the Seismological Society of America*, **106**, 1509-1517.

Laurendeau, A., Cotton, F., Ktenidou, O. J., Bonilla, L. F., Hollender, F. (2013). Rock and stiff-soil site amplification: Dependency on Vs30 and kappa (κ0). *Bulletin of the Seismological Society of America*, **103**, 3131-3148.

Laurendeau, A., Bard, P. Y., Hollender, F., Ktenidou, O. J., Foundotos, L., Hernandez, B., Perron, V. (2017). Towards the definition of reference motions (1000 ≤ Vs ≤ 3000 m/s): Analysis of the KiK-net data and correction of the local site effects. *Proceedings of the Sixteenth World Conference on Earthquake Engineering*, paper 4936, Santiago, Chile.

Lee, V. W., Trifunac, M. D. (2010). Should average shear-wave velocity in the top 30 m of soil be used to describe seismic amplification? *Soil Dynamics and Earthquake Engineering*, **30**, 1250-1258.

Lermo, J., Chávez-García, F. J. (1993). Site effect evaluation using spectral ratios with only one station. *Bulletin of the Seismological Society of America*, **83**, 1574-1594.

Madariaga, R. (1976). Dynamics of an expanding circular fault. *Bulletin of the Seismological Society of America*, **66**, 639-666.

Mayeda, K., Koyanagi, S., Hoshiba, M., Aki, K., Zeng, Y. (1992). A comparative study of scattering, intrinsic, and coda Q− 1 for Hawaii, Long Valley, and central California between 1.5 and 15.0 Hz. *Journal of Geophysical Research* , **97**, 6643-6659.

Mayor, J., Margerin, L., Calvet, M. (2014). Sensitivity of coda waves to spatial variations of absorption and scattering: radiative transfer theory and 2-D examples. *Geophysical Journal International*, **197**, 1117-1137.

Mayor, J., Calvet, M., Margerin, L., Vanderhaeghe, O., Traversa, P. (2016). Crustal structure of the Alps as seen by attenuation tomography. *Earth and Planetary Science Letters*, **439**, 71-80.

Mayor, J., Bora, S. S., Cotton, F. (2018a). Capturing regional variations of hard-rock κ0 from Coda analysis. *Bulletin of the Seismological Society of America*, **108**, 399-408.

Mayor, J., Traversa, P., Calvet, M., & Margerin, L. (2018b). Tomography of crustal seismic attenuation in Metropolitan France: implications for seismicity analysis. *Bulletin of Earthquake Engineering*, **16**, 2195-2210.

Moran, P. A. (1948). The interpretation of statistical maps. *Journal of the Royal Statistical Society. Series B (Methodological)*, **10**, 243-251.

Morasca, P., Malagnini, L., Akinci, A., Spallarossa, D., Herrmann, R. B. (2006). Ground-motion scaling in the western Alps. *Journal of Seismology*, **10**, 315-333.

Mucciarelli, M., Gallipoli, M. R. (2006). Comparison between Vs30 and other estimates of site amplification in Italy. *Proceedings of the First European Conference on Earthquake Engineering and Seismology*, Paper 270, Geneva, Switzerland.

Parolai, S. (2018). k0: Origin and Usability. *Bulletin of the Seismological Society of America*, **108**, 3446-3456.

Parolai, S., Bindi, D., Pilz, M. (2015). k0: The role of intrinsic and scattering attenuation. *Bulletin of the Seismological Society of America*, **105**, 1049-1052.

Parolai, S., Bindi, D. (2004). Influence of soil-layer properties on k evaluation. *Bulletin of the Seismological Society of America*, **94**, 349-356.

Perron, V., Laurendeau, A., Hollender, F., Bard, P. Y., Gélis, C., Traversa, P., Drouet, S. (2017). Selecting time windows of seismic phases and noise for engineering seismology applications: A versatile methodology and algorithm. *Bulletin of Earthquake Engineering*, doi: 10.1007/s10518-017-0131-9.

Petersen, M., Frankel, A., Harmsen, S., Mueller, C., Haller, K., Wheeler, R., Wesson, R., Zeng, Y., Boyd, O., Perkins, D., Luco, N., Field, E., Wills, C., Rukstales, K. (2008). Documentation for the 2008 update of the United States national seismic hazard maps , U.S. Geological Survey Open-File Report 2008-1128.

Pilz, M., & Fäh, D. (2017). The contribution of scattering to near-surface attenuation. *Journal of Seismology*, **21**, 837-855.

Poggi, V., Edwards, B., Fäh, D. (2011). Derivation of a reference shear-wave velocity model from empirical site amplification. *Bulletin of the Seismological Society of America*, **101**, 258-274.

Purvance, M. D., Anderson, J. G. (2003). A comprehensive study of the observed spectral decay in strong-motion accelerations recorded in Guerrero, Mexico. *Bulletin of the Seismological Society of America*, **93**, 600-611.

Rautian, T. G., Khalturin, V. I. (1978). The use of the coda for determination of the earthquake source spectrum. *Bulletin of the Seismological Society of America*, **68**, 923-948.

Richards, P. G., Menke, W. (1983). The apparent attenuation of a scattering medium. *Bulletin of the Seismological Society of America*, **73**, 1005-1021.

Rodriguez-Marek, A., Rathje, E. M., Bommer, J. J., Scherbaum, F., Stafford, P. J. (2014). Application of single-station sigma and site-response characterization in a probabilistic seismic-hazard analysis for a new nuclear site. *Bulletin of the Seismological Society of America*, **104**, 1601-1619.

Rodriguez-Marek, A., Kruiver, P. P., Meijers, P., Bommer, J. J., Dost, B., van Elk, J., Doornhof, D. (2017). A regional site-response model for the Groningen Gas Field. *Bulletin of the Seismological Society of America*, **107**, 2067-2077.

Roecker, S. W., Tucker, B., King, J., Hatzfeld, D. (1982). Estimates of Q in Central Asia as a function of frequency and depth using the coda of locally recorded earthquakes. *Bulletin of the Seismological Society of America*, **72**, 129-149.

Sato, H., Fehler, M. (1998). Scattering and attenuation of seismic waves in heterogeneous Earth. 332 pages, Springer Verlag, New York.

Scherbaum, F., Schmedes, J., Cotton, F. (2004). On the conversion of source-to-site distance measures for extended earthquake source models. *Bulletin of the Seismological Society of America*, **94**, 1053-1069.

Schneider, J. F., Silva, W. J., Stark, C. (1993). Ground motion model for the 1989 M 6.9 Loma Prieta earthquake including effects of source, path, and site. *Earthquake Spectra*, **9**, 251-287.

Shapiro, N. M., Campillo, M., Margerin, L., Singh, S. K., Kostoglodov, V., Pacheco, J. (2000). The energy partitioning and the diffusive character of the seismic coda. *Bulletin of the Seismological Society of America*, **90**, 655-665.

Silva, W. J., Abrahamson, N., Toro, G., Costantino, C. (1997). Description and validation of the stochastic ground motion model, Final Report, Brookhaven National Laboratory, Associated Universities, Inc. Upton, New York

Silva, W. J., Wong, I. G., Darragh, R. B., Rogers, A. M., Walsh, T. J., Kochelman, W. J., Priest, G. R. (1998). Engineering characterization of earthquake strong ground motions in the Pacific Northwest. *Assessing Earthquake Hazards and Reducing Risk in the Pacific Northwest*, 1560, 313-324.

Stanko, D., Markušić, S., Ivančić, I., Mario, G., Gülerce, Z. (2017). Preliminary estimation of Kappa parameter in Croatia. *IOP Conference Series: Earth and Environmental Science*, **95**, paper 032014, IOP Publishing, Bristol, United Kingdom.

Trifunac, M. D., Brady, A. G. (1975). A study on the duration of strong earthquake ground motion. *Bulletin of the Seismological Society of America*, **65**, 581-626.

Tsai, C. C. P., Chen, K. C. (2000). A model for the high-cut process of strong-motion accelerations in terms of distance, magnitude, and site condition: An example from the SMART 1 array, Lotung, Taiwan. *Bulletin of the Seismological Society of America*, **90**, 1535-1542.

Van Houtte, C., Drouet, S., Cotton, F. (2011). Analysis of the origins of κ (kappa) to compute hard rock to rock adjustment factors for GMPEs. *Bulletin of the Seismological Society of America*, **101**, 2926-2941.

Woessner, J., Laurentiu, D., Giardini, D., Crowley, H., Cotton, F., Grünthal, G., Valensise, G., Arvidsson, R., Basili, R., Demirciogli, M. B., Hiemer, S., Meletti, C., Musson, R. W., Rovida, A. N., Sesetyan, K., Stucchi, M. (2015). The 2013 European seismic hazard model: Key components and results. *Bulletin of Earthquake Engineering*, **13**, 3553-3596.

Zaccarelli, R., Bindi, D., Strollo, A., Quinteros, J., Cotton, F. (2019). Stream2segment: an open source tool for downloading, processing and visualizing massive event-based seismic waveform datasets, *Seismological Research Letters*, under review.

Zeng, Y. (1991). Compact solutions for multiple-scattered wave energy in time domain. *Bulletin of the Seismological Society of America*, **81**, 1022-1029.

Zhao, J. X., Irikura, K., Zhang, J., Fukushima, Y., Somerville, P. G., Asano, A., Ohno, Y., Oouchi, T., Takahashi, T., Ogawa, H. (2006). An empirical site-classification method for strong-motion stations in Japan using H/V response spectral ratio. *Bulletin of the Seismological Society of America*, **96**, 914-925.

Full mailing addresses of the authors

Marco Pilz, Fabrice Cotton, Riccardo Zaccarelli, Dino Bindi

Helmholtz Centre Potsdam – GFZ German Research Centre for Geosciences

Telegrafenberg

14467 Potsdam

Germany

Figure captions

Figure 1: East-west component of a recording of the 22 January 2014 M 4.2 recording at station Morigerati MGR in Italy. The onset of P, S and coda waves are indicated. The grey bands indicate the time windows for pre-event noise (A), S waves (B) and coda waves (C).

Figure 2: Example for the calculation of κ at site MGR using the event shown in Figure 1. The thin black line represents the Fourier acceleration spectrum while the grey line indicates the smoothened spectrum. The colored bands define the two frequency windows in which f_1 and f_2 are selected. Between these two bounds, all of the combinations of the slope of linear regression are tested. The straight colored lines represent minimum and maximum values of κ. The dotted line indicates the best in terms of the residuals of the regression (see text for further details). The color version of this figure is available only in the electronic edition.

Figure 3: Left: Location map of the 1384 seismic stations used in this study represented by colored triangles. Right: Magnitude-distance distribution. The color version of this figure is available only in the electronic edition.

Figure 4: κ_0^{coda} of all stations as a function of coda window length for different choices of the coda onset for T_{coda} = 20 s (left), T_{coda} = 40 s (middle) and $T_{\mathrm{coda}} = 2.3(T_S - T_P) + T_S$ (right, black lines) after the origin time of the earthquake. Epicentral distances range between 5 and 120 km. The red line represents the mean plus/minus one standard deviation. The color version of this figure is available only in the electronic edition.

Figure 5: Interpolated map of κ_0^{coda}. Stations are indicated as black dots. The color version of this figure is available only in the electronic edition.

Figure 6: Comparison of H/V spectral ratios of all sites considered being reference sites (black lines). The red line represents the mean plus/minus one standard deviation. The dashed lines indicate the frequency range for which the H/V spectral ratios have to be below a threshold of 2.5. The color version of this figure is available only in the electronic edition.

Figure 7: Estimates of κ_0^{AH} against κ_0^{coda} at reference sites (left) and non-reference sites (right).

Figure 8: κ_0^{coda} against magnitude bins (bin width 0.5 units). The mean of each magnitude bin is indicated as circles with plus/minus one standard deviation.

Figure 9: Scatter plot of interpolated κ_0^{coda} at reference sites from Figure 5 against measured κ_0^{AH} at reference sites for the computation of the correlation coefficient.

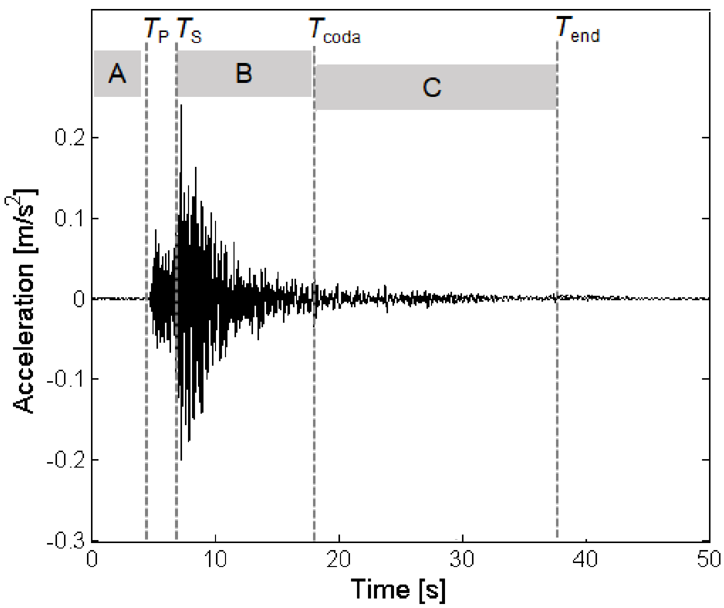

Figure 1: East-west component of a recording of the 22 January 2014 M 4.2 recording at station Morigerati MGR in Italy. The onset of P, S and coda waves are indicated. The grey bands indicate the time windows for pre-event noise (A), S waves (B) and coda waves (C).

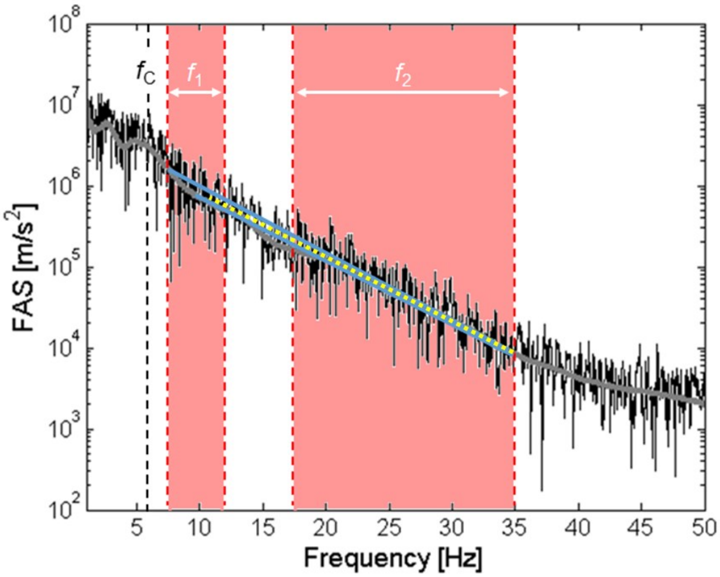

Figure 2: Example for the calculation of κ at site MGR using the event shown in Figure 1. The thin black line represents the Fourier acceleration spectrum while the grey line indicates the smoothened spectrum. The colored bands define the two frequency windows in which f_1 and f_2 are selected. Between these two bounds, all of the combinations of the slope of linear regression are tested. The straight colored lines represent minimum and maximum values of κ. The dotted line indicates the best in terms of the residuals of the regression (see text for further details). The color version of this figure is available only in the electronic edition.

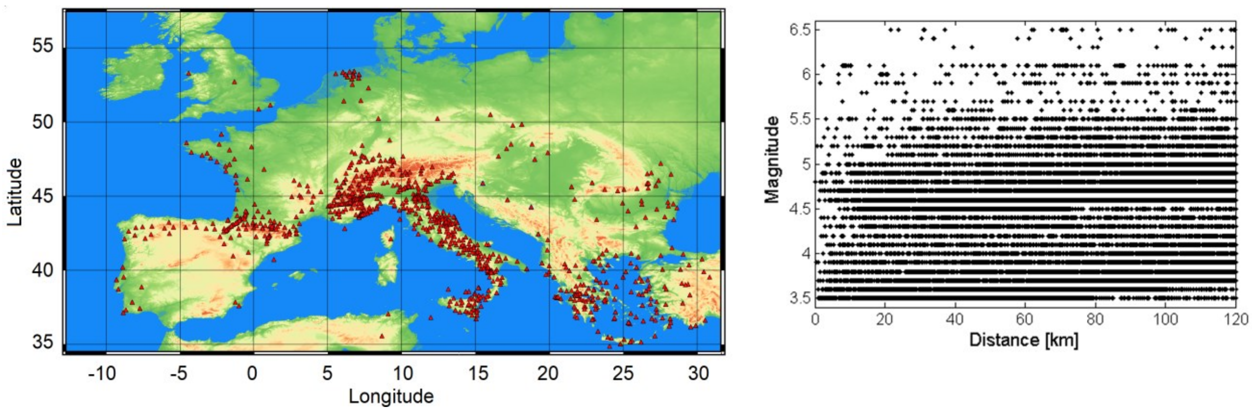

Figure 3: Left: Location map of the 1384 seismic stations used in this study represented by colored triangles. Right: Magnitude-distance distribution. The color version of this figure is available only in the electronic edition.

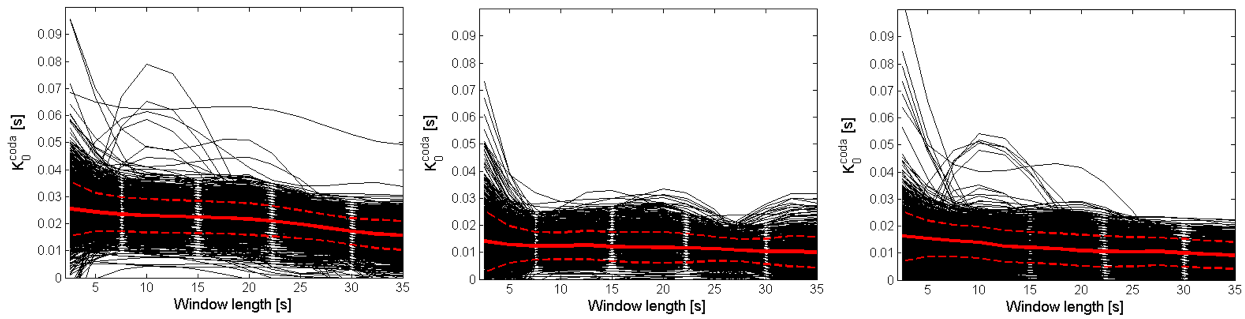

Figure 4: κ_0^{coda} of all stations as a function of coda window length for different choices of the coda onset for $T_{\mathrm{coda}} = 20$ s (left), $T_{\mathrm{coda}} = 40$ s (middle) and $T_{\mathrm{coda}} = 2.3(T_S - T_P) + T_S$ (right, black lines) after the origin time of the earthquake. Epicentral distances range between 5 and 120 km. The red line represents the mean plus/minus one standard deviation. The color version of this figure is available only in the electronic edition.

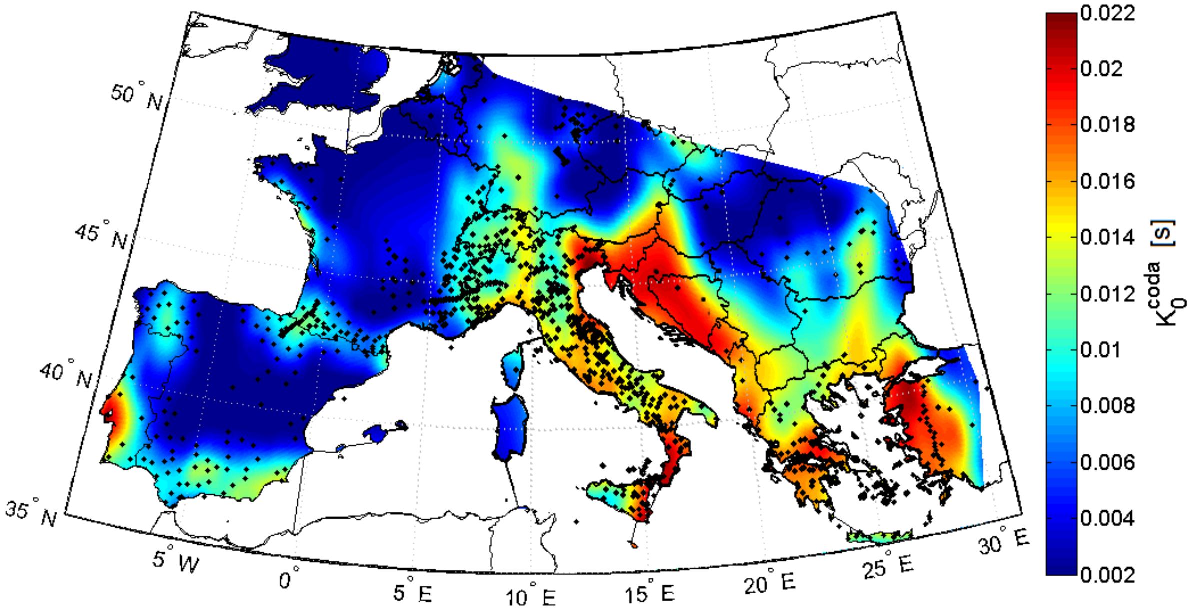

Figure 5: Interpolated map of κ_0^{coda}. Stations are indicated as black dots. The color version of this figure is available only in the electronic edition.

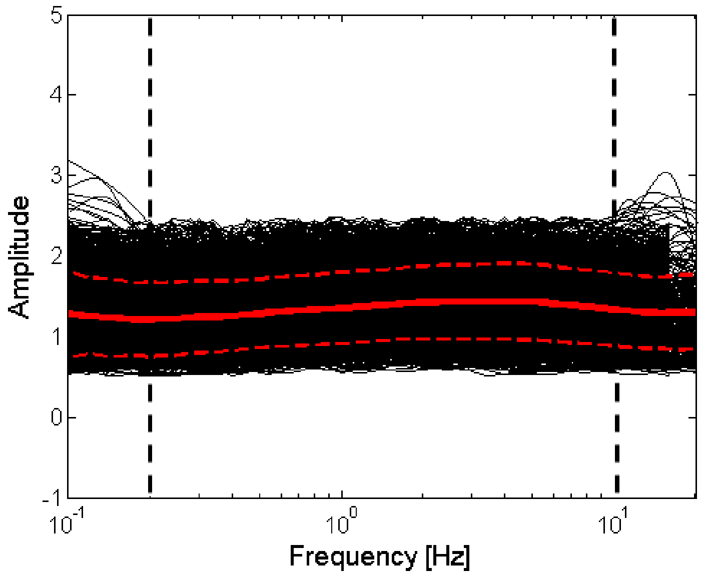

Figure 6: Comparison of H/V spectral ratios of all sites considered being reference sites (black lines). The red line represents the mean plus/minus one standard deviation. The dashed lines indicate the frequency range for which the H/V spectral ratios have to be below a threshold of 2.5. The color version of this figure is available only in the electronic edition.

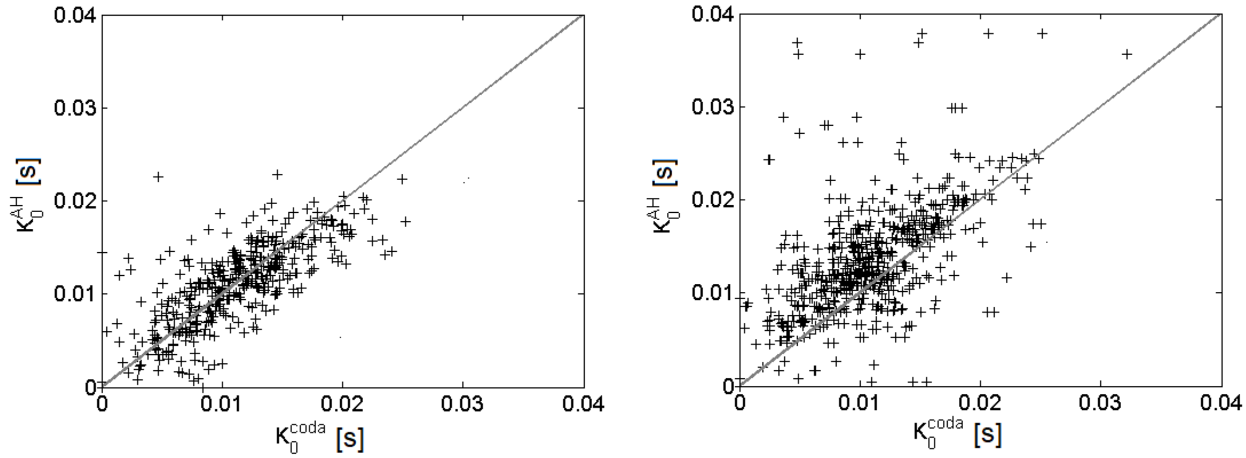

Figure 7: Estimates of κ_0^{AH} against κ_0^{coda} at reference sites (left) and non-reference sites (right).

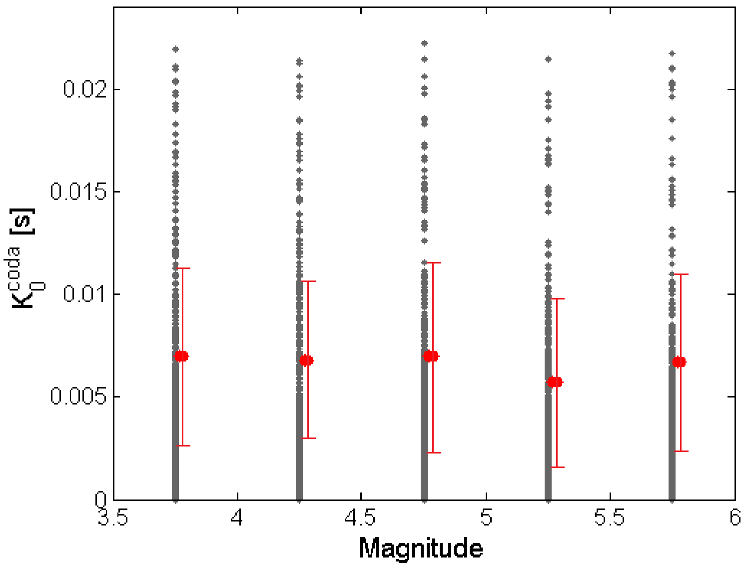

Figure 8: κ_0^{coda} against magnitude bins (bin width 0.5 magnitude units). The mean of each magnitude bin is indicated as circles with plus/minus one standard deviation.

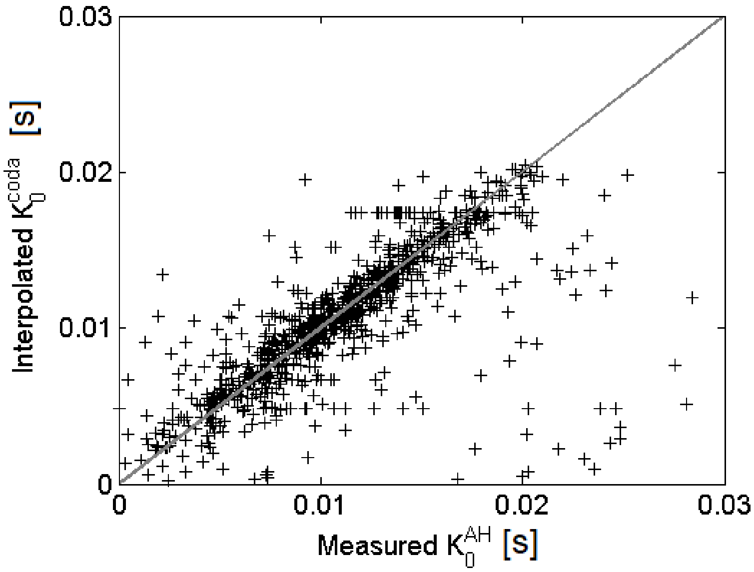

Figure 9: Scatter plot of interpolated κ_0^{coda} at reference sites from Figure 5 against measured κ_0^{AH} at reference sites for the computation of the correlation coefficient.

Appendix A1

List of 717 stations indicated as reference sites.

Station	Network	Lat [°]	Lon [°]	Start	End	κ_0^{coda} [s]
ABSI	SI	46.7285 N	11.3205 E	2006		0.0078
ACER	IV	40.7867 N	15.9427 E	2007		0.0096
ACOM	NI / OX	46.5480 N	13.5137 E	2005		0.0063
AGG	HT	39.0211 N	22.3360 E	2007		0.0135
AGRP	CL	38.3959 N	21.7228 E	2012		0.0111
AIGLE	CH	46.3418 N	6.9530 E	1998		0.0100
AIO	MN / IV	37.9712 N	15.2330 E	2012		0.0110
ALJA	IV	37.7490 N	13.7537 E	2008		0.0089
ALN	HT	40.8850 N	26.0460 E	2007		0.0098
AMGA	HL	36.8316 N	25.8938 E	2012		0.0096
AMUR	IV	40.9071 N	16.6041 E	2005		0.0120
ANKY	HL	35.8670 N	23.3012 E	2010		0.0099
ANTF	FR	43.5644 N	7.1234 E	2003	2013	0.0062
AOI	IV	43.5502 N	13.6020 E	2004		0.0116
AOS	HT	39.1654 N	23.8639 E	2008	2018	0.0120
APE	GE / HL	37.0727 N	25.5230 E	2000		0.0097
AQU	MN / IV	42.3540 N	13.4050 E	1988		0.0101
ARG	HL	36.2136 N	28.1212 E	2003		0.0111
ARVD	IV	43.4981 N	12.9415 E	2003		0.0138
ASQU	IV	43.7967 N	11.7893 E	2007		0.0098
ASSB	IV	43.0426 N	12.6587 E	2008		0.0109
ASTA	HL	36.5455 N	26.3530 E	2011		0.0109
ATCA	IV	43.5659 N	12.2661 E	2010	2013	0.0124
ATE	FR	43.0858 N	0.7003 W	1995		0.0060
ATFO	IV	43.3666 N	12.5715 E	2009		0.0120
ATHU	HA	37.9665 N	23.7845 E	2007		0.0114
ATLO	IV	43.3152 N	12.4073 E	2009		0.0111
ATMI	IV	43.3342 N	12.2680 E	2009		0.0116
ATPC	IV	43.4807 N	12.4570 E	2009		0.0121
ATTE	IV	43.1979 N	12.3536 E	2009		0.0130
ATVO	IV	43.3821 N	12.4066 E	2009		0.0150
AVR	MT	44.9558 N	5.6531 E	2007		0.0044

BAG8	IV	45.8228 N	10.4664 E	2010		0.0056
BALST	CH	47.3358 N	7.6950 E	2000		0.0061
BDI	IV	44.0628 N	10.5956 E	2003		0.0087
BERGE	CH	47.8716 N	8.1780 E	2012		0.0061
BERNI	CH	46.4136 N	10.0231 E	1998		0.0136
BIBA	CH	46.3025 N	7.9304 E	2009		0.0076
BNALP	CH	46.8703 N	8.4249 E	1998		0.0116
BNI	MN	45.0520 N	6.6780 E	1988		0.0069
BOB	IV	44.7679 N	9.4478 E	2003		0.0102
BOBI	CH	47.5463 N	8.3398 E	2013		0.0065
BOTT	IV	45.5494 N	10.3095 E	2009	2014	0.0077
BOURR	CH	47.3936 N	7.2301 E	1998		0.0061
BRANT	CH	46.9380 N	6.4730 E	2002		0.0061
BSSO	IV	41.5461 N	14.5938 E	2005		0.0085
BSTF	FR	43.8009 N	5.6433 E	2010		0.0028
BUD	HU	47.4831 N	19.0201 E	2004		0.0085
CADA	IV	43.1942 N	13.7614 E	2010		0.0087
CAFE	IV	41.0280 N	15.2366 E	2005		0.0094
CAFI	IV	43.3292 N	11.9663 E	2007		0.0110
CAFR	IV	42.2273 N	14.3470 E	2005	2017	0.0062
CAGR	IV	37.6220 N	14.4999 E	2010		0.0102
CALF	FR	43.7528 N	6.9218 E	1995		0.0064
CANF	LC	42.7637 N	0.5175 W	2011		0.0047
CASP	IV	42.7908 N	10.8652 E	2007		0.0092
CBRU	CA	42.2855 N	2.1803 E	2000		0.0035
CDRU	IV	40.4896 N	15.3046 E	2005		0.0145
CEL	MN	38.2603 N	15.8939 E	2003		0.0157
CELI	IV	39.4027 N	16.5088 E	2011		0.0130
CERA	IV	41.5978 N	14.0183 E	2006		0.0097
CERT	IV	41.9490 N	12.9818 E	2003		0.0134
CESX	IV	42.6085 N	12.5868 E	2008		0.0079
CET2	IV	39.5288 N	15.9546 E	2011		0.0129
CHIF	FR	46.1335 N	0.4077 W	2000		0.0021
CHMF	FR	47.2484 N	6.6517 E	2009		0.0062
CHOS	HT	38.3869 N	26.0506 E	2006		0.0163
CIGN	IV	41.6542 N	14.9050 E	2003		0.0088
CIMA	IV	43.3053 N	13.6701 E	2010		0.0138
CING	IV	43.3756 N	13.1954 E	2003		0.0121
CIRO	GU	45.6019 N	7.5682 E	2010		0.0088
CLTA	IV	37.1580 N	13.9620 E	2012		0.0077
CMPR	IV	40.3181 N	15.3030 E	2005		0.0092

COR1	IV	43.6318 N	13.0003 E	2011		0.0092
CORL	IV	37.8943 N	13.3038 E	2006		0.0117
CRE	IV	43.6189 N	11.9517 E	2003		0.0098
CRMI	IV	43.7956 N	10.9795 E	2006		0.0111
CSA1	4A	39.8403 N	15.9300 E	2012	2014	0.0147
CSA2	4A	39.8422 N	15.9276 E	2012	2014	0.0148
CSA3	4A	39.8396 N	15.9265 E	2012	2014	0.0110
CSA4	4A	39.8403 N	15.9254 E	2012	2014	0.0111
CSA5	4A	39.8420 N	15.9262 E	2012	2014	0.0085
CSB	4A	39.8153 N	16.1677 E	2012	2014	0.0114
CSB	Y4	39.8153 N	16.1678 E	2014	2015	0.0114
CSC	4A	40.0083 N	15.9762 E	2012	2014	0.0082
CT07	YP	44.4105 N	5.5170 E	2012	2013	0.0024
CT08	YP	44.4119 N	5.6051 E	2012	2013	0.0028
CT09	YP	44.4295 N	5.7144 E	2012	2013	0.0033
CT12	YP	44.4751 N	5.9826 E	2012	2013	0.0050
CT13	YP	44.4596 N	6.0559 E	2012	2013	0.0050
CT14	YP	44.4609 N	6.1375 E	2012	2013	0.0055
CT15	YP	44.4693 N	6.2362 E	2012	2013	0.0064
CT16	YP	44.4771 N	6.3140 E	2012	2013	0.0062
CT17	YP	44.5041 N	6.3576 E	2012	2013	0.0065
CT18	YP	44.5006 N	6.4555 E	2012	2013	0.0069
CT19	YP	44.5409 N	6.5198 E	2012	2013	0.0095
CT22	YP	44.6663 N	6.6248 E	2012	2013	0.0077
CT23	YP	44.6642 N	6.6848 E	2012	2013	0.0074
CT24	YP	44.7288 N	6.7449 E	2012	2013	0.0073
CT25	YP	44.7255 N	6.7705 E	2012	2013	0.0073
CT26	YP	44.7650 N	6.8042 E	2012	2013	0.0091
CT27	YP	44.7662 N	6.8799 E	2012	2013	0.0073
CT28	YP	44.7954 N	6.9237 E	2012	2013	0.0072
CT30	YP	44.7732 N	7.0393 E	2012	2013	0.0074
CT31	YP	44.7982 N	7.0814 E	2012	2013	0.0073
CT32	YP	44.8091 N	7.1301 E	2012	2013	0.0073
CT33	YP	44.8250 N	7.2010 E	2012	2013	0.0073
CT38	YP	45.0186 N	7.7484 E	2012	2013	0.0064
CT40	YP	45.0693 N	7.9170 E	2012	2013	0.0061
CT41	YP	45.0866 N	8.0426 E	2012	2013	0.0061
CT42	YP	45.0990 N	8.1729 E	2012	2013	0.0063
CT44	YP	45.0657 N	8.4265 E	2012	2013	0.0070
CT45	YP	45.0441 N	8.5425 E	2012	2013	0.0072
CT46	YP	44.9890 N	8.6687 E	2012	2013	0.0078

CT47	YP	43.9285 N	5.1865 E	2012	2013	0.0019
CT49	YP	44.1803 N	6.6246 E	2012	2013	0.0067
CT50	YP	44.5620 N	7.3201 E	2012	2013	0.0083
CT52	YP	45.0359 N	6.4000 E	2012	2013	0.0069
CTRE	CA	42.3242 N	0.7736 E	2006	2035	0.0033
CUC	MN	39.9938 N	15.8155 E	2003		0.0117
DAGMA	CH	47.2309 N	8.0125 E	2013		0.0067
DAVOX	CH	46.7805 N	9.8795 E	2002		0.0110
DID	HP	37.5063 N	23.2368 E	2007		0.0143
DID	XY	37.5063 N	23.2368 E	2008	2009	0.0143
DIX	CH	46.0811 N	7.4084 E	1976		0.0055
DOI	IV	44.5042 N	7.2466 E	2003	2015	0.0084
DRO	HP	37.9520 N	21.7100 E	2010		0.0159
DSF	HP	38.4112 N	22.5271 E	2008		0.0126
E018	IB	37.9803 N	5.9548 W	2007	2009	0.0018
E025	IB	37.7016 N	3.4657 W	2007	2009	0.0042
E030	IB	38.4684 N	5.6264 W	2007	2009	0.0013
E034	IB	38.2298 N	2.1918 W	2008	2009	0.0057
E041	IB	38.6500 N	3.6572 W	2009	2010	0.0032
E051	IB	38.9925 N	3.6714 W	2009	2010	0.0024
E056	IB	39.1320 N	0.6447 W	2009	2010	0.0012
E060	IB	39.7615 N	4.6337 W	2009	2010	0.0085
E062	IB	39.6400 N	2.5312 W	2009	2011	0.0009
E064	IB	39.6554 N	1.4590 W	2009	2010	0.0085
E074	IB	40.1312 N	2.4199 W	2009	2011	0.0085
E085	IB	40.4993 N	1.9736 W	2009	2011	0.0085
E086	IB	40.5569 N	1.0970 W	2009	2010	0.0085
E138	IB	42.8515 N	7.9689 W	2010	2013	0.0057
E139	IB	42.9373 N	7.5104 W	2011	2013	0.0051
E140	IB	42.9504 N	6.8722 W	2010	2013	0.0031
E143	IB	42.9062 N	4.6081 W	2010	2014	0.0066
E145	IB	42.7966 N	3.2075 W	2011	2014	0.0063
E149	IB	42.7637 N	0.5175 W	2011	2013	0.0048
E153	IB	43.2292 N	5.7227 W	2011	2014	0.0025
E154	IB	43.3519 N	4.6015 W	2011	2014	0.0048
E155	IB	43.2448 N	3.9987 W	2010	2014	0.0052
E157	IB	43.1707 N	2.1283 W	2011	2013	0.0022
E158	IB	42.6608 N	0.1906 E	2011	2012	0.0045
ECH	G	48.2163 N	7.1590 E	1990		0.0061
ECHE	IB	39.5896 N	0.9690 W	2009	2010	0.0085
ECNV	IV	37.5956 N	14.7125 E	2007	2017	0.0115

EDMD	GB	54.8312 N	1.9636 W	2011		0.0017
EFSA	HL	39.5401 N	24.9886 E	2010		0.0088
EILF	FR	43.5479 N	7.1312 E	2011		0.0058
EJON	ES	42.4487 N	2.8886 E	2000		0.0065
ELOJ	IB	37.1464 N	4.1540 W	2007	2009	0.0046
EMBD	CH	46.2165 N	7.8322 E	2009		0.0049
EMING	CH	47.8952 N	8.8468 E	2013		0.0073
EMMET	CH	47.4376 N	8.0136 E	2012		0.0064
EMV	CH	46.0632 N	6.8988 E	1981	2012	0.0063
ENR	GU	44.2267 N	7.4203 E	2011		0.0092
EOSO	ES	28.0718 N	15.552 W	2000		0.0090
EPID	HA	37.6144 N	23.1189 E	2011		0.0138
EQUI	GU	44.1660 N	10.1530 E	2012		0.0081
EREA	HA	38.4199 N	23.9318 E	2010		0.0107
ESCA	FR	43.8310 N	7.3744 E	2003		0.0081
ESLN	IV	37.6934 N	14.9744 E	2005		0.0100
EVGI	HT	38.6210 N	20.6560 E	2012		0.0124
EVO	G	38.5320 N	8.0130 W	1996	2000	0.0085
EVO	WM	38.5294 N	8.0167 W	2006		0.0085
EVR	HL	38.9166 N	21.8105 E	2010		0.0112
EVRN	IV	37.6892 N	15.1356 E	2010		0.0140
EWZT0	CH	47.3668 N	8.4968 E	2009		0.0068
EZAM	IB	42.1482 N	8.6968 W	2010	2012	0.0039
FAGN	IV	42.2657 N	13.5838 E	2004		0.0082
FAVR	IV	37.2671 N	13.6670 E	2003		0.0063
FDMO	IV	43.0365 N	13.0873 E	2008		0.0088
FEMA	IV	42.9621 N	13.0498 E	2009		0.0104
FIAM	IV	42.2680 N	13.1172 E	2004		0.0139
FIESA	CH	46.4352 N	8.1105 E	2009		0.0080
FILT	YX	38.4493 N	21.9656 E	2002	2002	0.0150
FIR	IV	43.7744 N	11.2551 E	2009		0.0079
FIR	Y4	44.7936 N	6.0022 E	2004	2007	0.0043
FIU1	IV	43.1886 N	12.9316 E	2011		0.0114
FIVI	GU	44.2393 N	10.1273 E	2008		0.0136
FNVD	IV	44.1678 N	11.1229 E	2003		0.0108
FODE	GE	35.3797 N	24.9576 E	2000	2003	0.0098
FOEL	GB	52.8879 N	3.2012 W	2008		0.0027
FRE8	IV	46.0150 N	12.3552 E	2011		0.0141
FRES	IV	41.9735 N	14.6693 E	2004		0.0090
FROS	IV	43.2097 N	11.1562 E	2010		0.0122
FSK	HP	38.4593 N	20.5623 E	2012		0.0130

FSSB	IV	43.6931 N	12.7771 E	2003		0.0111
FULLY	CH	46.1563 N	7.1358 E	2018		0.0071
FUORN	CH	46.6203 N	10.2636 E	2000		0.0098
FUSIO	CH	46.4548 N	8.6629 E	1999		0.0068
FVI	IV	46.5966 N	12.7804 E	2003		0.0141
GALF	IV	37.7107 N	14.5665 E	2006		0.0071
GATE	IV	41.5131 N	14.9102 E	2009		0.0113
GBAS	SL	45.9348 N	14.4434 E	2008		0.0130
GBRS	SL	45.5311 N	14.8101 E	2007		0.0138
GCIS	SL	45.8672 N	15.6275 E	2003		0.0138
GEC2	GR	48.8443 N	13.7006 E	1997		0.0085
GIB	IV	37.9901 N	14.0260 E	2003		0.0091
GIMEL	CH	46.5336 N	6.2655 E	1999		0.0058
GIUL	IV	41.5583 N	13.2546 E	2003		0.0136
GRC1	GR	48.9962 N	11.5214 E	1978		0.0020
GRC2	GR	48.8676 N	11.3755 E	1978		0.0020
GRC3	GR	48.8902 N	11.5858 E	1978		0.0014
GRC4	GR	49.0867 N	11.5263 E	1978		0.0019
GRFO	IU	49.6909 N	11.2203 E	1994		0.0027
GRG	HT	40.9570 N	22.4010 E	2008		0.0082
GRIMS	CH	46.5781 N	8.3189 E	2011		0.0079
GROG	IV	43.4262 N	9.8920 E	2005	2018	0.0095
GROS	SL	46.4610 N	15.5018 E	2002		0.0128
GRYON	CH	46.2505 N	7.1111 E	2002		0.0072
GRZ1	TH	50.6908 N	12.2196 E	2012		0.0027
GTTG	GR	51.5464 N	9.9642 E	2003		0.0013
GUAR	IV	41.7945 N	13.3123 E	2003		0.0078
GUNZ	SX	50.3635 N	12.3316 E	2003		0.0031
GUT	CH	48.0707 N	9.1153 E	1997	2009	0.0080
GVD	GE	34.8392 N	24.0873 E	1999	2003	0.0055
GVD	GE	34.8391 N	24.0874 E	2003		0.0055
GVD	HL	34.8391 N	24.0874 E	2010		0.0055
HAGA	IV	37.2850 N	15.1550 E	2006		0.0121
HAMIK	CH	47.2451 N	8.2706 E	2013		0.0067
HASLI	CH	46.7568 N	8.1512 E	1999		0.0074
HAVL	IV	36.9596 N	15.1220 E	2005	2017	0.0154
HBSP	IV	37.1270 N	14.4920 E	2012	2018	0.0114
HCRL	IV	37.2831 N	15.0325 E	2008	2017	0.0171
HLNI	IV	37.3485 N	14.8720 E	2009		0.0131
HMDC	IV	36.9590 N	14.7831 E	2005		0.0185
HORT	HT	40.5978 N	23.0996 E	2008		0.0071

HSKC	7E	50.6073 N	13.4315 E	2006	2008	0.0085
HSKC	CZ	50.6072 N	13.4317 E	2014		0.0085
HVZN	IV	37.1783 N	14.7155 E	2005		0.0148
IACL	IV	38.5330 N	14.3550 E	2007		0.0115
IACM	HL	35.3058 N	25.0709 E	2010		0.0127
IDI	HL	35.2880 N	24.8900 E	2010		0.0088
IDI	MN	35.2880 N	24.8900 E	1994		0.0088
IFIL	IV	38.5642 N	14.5753 E	2005		0.0120
IGT	HT	39.5315 N	20.3299 E	2008		0.0108
IKRA	HL	37.6112 N	26.2928 E	2010		0.0098
ILLEZ	CH	46.2193 N	6.9404 E	2017		0.0068
ILLI	IV	38.4457 N	14.9483 E	2005		0.0120
IMMV	GE	35.4606 N	23.9811 E	2010		0.0084
IMMV	HL	35.4606 N	23.9811 E	2010		0.0084
IMTC	IV	40.7209 N	13.8758 E	1988		0.0102
INTR	IV	42.0115 N	13.9046 E	2003		0.0122
IOAT	YX	38.3459 N	22.2729 E	2002	2002	0.0126
IOCA	IV	40.7458 N	13.9008 E	1988		0.0102
ISO	FR	44.1840 N	7.0500 E	1995		0.0073
ISO	ZO	46.1450 N	12.0780 E	2002	2003	0.0128
IST3	IV	38.7992 N	15.2304 E	2012		0.0148
JAN	HL	39.6562 N	20.8487 E	2010		0.0134
JAUN	CH	46.6340 N	7.2910 E	2018		0.0073
JOPP	IV	38.6068 N	15.8856 E	2006		0.0207
KALE	HA	38.3911 N	22.1398 E	2007		0.0155
KARP	GE	35.5471 N	27.1611 E	2009		0.0106
KARP	HL	35.5471 N	27.1611 E	2003		0.0106
KASA	HL	39.7463 N	19.9354 E	2010		0.0133
KAVA	HT	40.9967 N	24.5137 E	2008		0.0091
KEK	HL	39.7127 N	19.7962 E	2003		0.0136
KEK	MN	39.7127 N	19.7962 E	2000		0.0136
KOSI	SI	46.4630 N	11.3778 E	2006		0.0085
KOSI	Z3	36.7449 N	26.9517 E	2005	2007	0.0130
KSL	HL	36.1503 N	29.5856 E	2010		0.0055
LAUCH	CH	46.4155 N	7.7717 E	2010		0.0079
LAVEY	CH	46.2000 N	7.0228 E	2017		0.0070
LIENZ	CH	47.2946 N	9.4927 E	2004		0.0118
LIT	HT	40.1033 N	22.4892 E	2006		0.0097
LKBD	CH	46.3870 N	7.6271 E	1999	2017	0.0074
LKBD2	CH	46.3746 N	7.6443 E	2001		0.0080
LKD	HT	38.7072 N	20.6506 E	2006	2008	0.0122

LKD2	HT	38.7889 N	20.6578 E	2008		0.0107
LKR	HL	38.6496 N	22.9989 E	2010		0.0185
LKR	XY	38.6500 N	23.0000 E	2007	2009	0.0185
LLS	CH	46.8468 N	9.0082 E	1978		0.0067
LMK	GB	53.4573 N	0.3274 W	2009		0.0085
LNSS	IV	42.6029 N	13.0403 E	2004		0.0132
LOUT	HA	37.9879 N	22.9743 E	2010		0.0125
LPEL	IV	42.0468 N	14.1832 E	2008		0.0094
LRVF	FR	44.9478 N	0.3100 W	2011		0.0024
LSD	GU	45.4595 N	7.1343 E	2007		0.0070
LTK	HP	38.0228 N	22.9673 E	2006		0.0112
LTRZ	IV	40.6032 N	16.8191 E	2003		0.0106
LUSI	SI	45.9595 N	10.9436 E	2012		0.0059
MA9	IV	41.7698 N	12.6591 E	2008		0.0115
MABI	IV	46.0549 N	10.5140 E	2003		0.0070
MACI	IU	28.2502 N	16.508 W	2008		0.0091
MAGA	IV	45.7753 N	10.6286 E	2006		0.0064
MAKT	YX	38.4331 N	22.1248 E	2002	2002	0.0131
MAON	IV	42.4283 N	11.1309 E	2003		0.0108
MATE	GE	40.6491 N	16.7044 E	2007		0.0119
MCH1	GB	51.9973 N	2.9983 W	2004		0.0028
MCIV	IV	42.7786 N	11.6765 E	2010		0.0150
MCPD	IV	38.1199 N	14.7310 E	2012	2018	0.0118
MCRV	IV	40.7826 N	15.1684 E	2005		0.0107
MCSR	IV	38.0646 N	15.2301 E	2010	2017	0.0105
MDAR	IV	43.1927 N	13.1427 E	2008		0.0082
MDI	IV	45.7697 N	9.7160 E	2004		0.0141
ME12	IV	38.6315 N	15.0700 E	2007	2010	0.0123
MEF	HE	60.2172 N	24.3958 E	2006		0.0021
MELA	IV	41.7059 N	15.1270 E	2008		0.0126
MERA	IV	45.7054 N	9.4291 E	2009		0.0094
MESG	IV	40.5894 N	17.8504 E	2009		0.0076
MESJ	LX	37.8395 N	8.2199 W	2007		0.0085
METMA	CH	47.7122 N	8.2526 E	2013		0.0063
MFSFA	CH	46.5004 N	8.8080 E	2005	2011	0.0082
MFSFB	CH	46.5055 N	8.8045 E	2006	2009	0.0082
MGAB	IV	42.9126 N	12.1121 E	2008		0.0109
MGNA	HL	38.6561 N	20.7912 E	2010		0.0125
MGR	IV	40.1376 N	15.5535 E	2003		0.0102
MHLA	HL	36.7450 N	24.4219 E	2011	2015	0.0091
MHLO	HL	36.6898 N	24.4017 E	2010		0.0091

MIDA	IV	41.6419 N	14.2540 E	2004		0.0120
MIGL	IV	40.6044 N	16.4410 E	2006		0.0105
MIL	7E	50.5403 N	13.9357 E	2006	2008	0.0085
MIL	XY	36.7083 N	24.5322 E	2007	2009	0.0096
MILE	ZZ	36.7320 N	24.4990 E	2002	2003	0.0083
MILN	IV	45.4803 N	9.2321 E	2012		0.0088
MILN	ZZ	36.7580 N	24.4230 E	2002	2003	0.0088
MILO	ZZ	36.6900 N	24.4020 E	2002	2003	0.0091
MILS	ZZ	36.6930 N	24.5030 E	2002	2003	0.0094
MLS	FR	42.9560 N	1.0950 E	1995		0.0052
MLYF	FR	43.9880 N	5.7675 E	2010		0.0032
MMK	CH	46.0507 N	7.9641 E	1981		0.0067
MMME	IV	37.9352 N	15.2539 E	2004	2012	0.0133
MMN	IV	39.8910 N	15.9904 E	2009		0.0178
MMUR	IV	43.4418 N	12.9973 E	2008		0.0087
MNS	IV	42.3855 N	12.6811 E	2003	2013	0.0105
MNT3	IX	40.8370 N	15.0067 E	2006		0.0088
MNTP	IV	43.1374 N	13.4693 E	2012		0.0100
MNVA	HL	36.6871 N	23.0373 E	2010		0.0084
MOCO	IV	41.3700 N	15.1580 E	2005		0.0070
MONC	IV	45.0739 N	7.9271 E	2005		0.0072
MORC	CZ	49.7766 N	17.5428 E	1993		0.0067
MORC	GE	49.7766 N	17.5428 E	1993		0.0067
MORC	M1	49.7768 N	17.5425 E	2012		0.0067
MOSI	SI	46.6164 N	10.5495 E	2006		0.0060
MPAG	IV	43.6292 N	12.7595 E	2009		0.0125
MPNC	IV	38.1465 N	15.3528 E	2010		0.0210
MRB1	IV	41.1227 N	14.9682 E	2003		0.0089
MRKA	HA	38.7047 N	23.5847 E	2008		0.0129
MRVN	IV	41.0609 N	16.1958 E	2007		0.0106
MSCL	IV	38.2320 N	15.7900 E	2007		0.0199
MSFR	IV	38.0339 N	14.5916 E	2011		0.0110
MSRU	IV	38.2639 N	15.5083 E	2004		0.0196
MSSA	IV	44.3162 N	9.5174 E	2008		0.0111
MTCE	IV	42.0228 N	12.7422 E	2003		0.0106
MTI01	CH	47.3791 N	7.1654 E	2014		0.0063
MTI02	CH	47.3793 N	7.1652 E	2014		0.0063
MTIA1	CH	47.3798 N	7.1648 E	2014		0.0063
MTIA2	CH	47.3718 N	7.1715 E	2014		0.0063
MTIA3	CH	47.3703 N	7.1237 E	2015		0.0064
MTIA4	CH	47.3850 N	7.2004 E	2015		0.0062

MTRZ	IV	44.3128 N	11.4248 E	2007		0.0076
MTSN	IV	40.2663 N	15.7515 E	2006		0.0114
MTTG	IV	38.0031 N	15.6999 E	2003		0.0131
MUCR	IV	38.0430 N	14.8739 E	2011		0.0183
MUGIO	CH	45.9219 N	9.0417 E	2001		0.0076
MUO	CH	46.9676 N	8.6371 E	1981		0.0083
NALPS	CH	46.5951 N	8.7483 E	2011		0.0083
NARO	IV	43.6108 N	12.5806 E	2011		0.0161
NEO	HL	39.3057 N	23.2219 E	2010		0.0139
NOV	IV	38.0278 N	15.1367 E	2007		0.0159
NPS	HL	35.2613 N	25.6104 E	2010		0.0097
NSC3	IX	40.8468 N	15.1222 E	2012		0.0090
NVR	HL	41.3485 N	23.8652 E	2010		0.0089
OFFI	IV	42.9350 N	13.6857 E	2006		0.0112
OG02	FR	46.1542 N	6.2202 E	2011		0.0059
OG35	FR	46.0448 N	5.5718 E	2010		0.0032
OGAG	FR	44.7878 N	6.5397 E	1995		0.0088
OGDI	FR	44.1093 N	6.2253 E	1995		0.0054
OGGM	FR	45.2057 N	6.1167 E	1995		0.0059
OGMO	FR	45.2086 N	6.6831 E	1996		0.0076
OGS2	FR	45.0648 N	5.8020 E	2012		0.0035
OGSM	FR	45.6093 N	5.6972 E	2011		0.0048
OKC	CZ	49.8346 N	18.1400 E	1998		0.0114
OSSC	IV	43.5236 N	11.2458 E	2011		0.0092
OTER1	CH	47.5778 N	7.6039 E	2006		0.0055
OUR	HT	40.3325 N	23.9791 E	2008		0.0104
PANIX	CH	46.8257 N	9.1117 E	2011		0.0095
PARC	IV	43.6486 N	12.2386 E	2008		0.0117
PATC	HL	38.2693 N	21.7600 E	2010		0.0124
PCP	GU	44.5413 N	8.5452 E	2006		0.0136
PE03	X7	42.6379 N	1.2492 E	2011	2012	0.0042
PE03	Z3	37.3784 N	21.7722 E	2005	2007	0.0157
PE05	X7	42.5758 N	1.2122 E	2011	2012	0.0043
PE05	Z3	37.5128 N	22.4553 E	2005	2007	0.0099
PE06	X7	42.5350 N	1.2616 E	2011	2012	0.0042
PE06	Z3	37.1787 N	21.9252 E	2005	2007	0.0116
PE16	X7	42.1536 N	0.9534 E	2011	2012	0.0028
PESA	IV	43.9410 N	12.8402 E	2003		0.0197
PF01	X7	42.7589 N	1.1883 E	2011	2012	0.0044
PF04	X7	42.9023 N	1.2103 E	2011	2012	0.0044
PF05	X7	42.9255 N	1.2361 E	2011	2012	0.0042

PF07	X7	43.0089 N	1.2683 E	2011	2012	0.0040
PF08	X7	43.0583 N	1.2667 E	2011	2012	0.0037
PF09	X7	43.0972 N	1.3070 E	2011	2012	0.0033
PFVI	PM	37.1328 N	8.8268 W	2008		0.0085
PIEI	IV	43.5357 N	12.5350 E	2003		0.0156
PIGN	IV	41.2000 N	14.1799 E	2011		0.0100
PIO1	IV	43.1782 N	12.9838 E	2011		0.0114
PIPA	IV	39.4851 N	16.8158 E	2008		0.0156
PLAC	IV	38.4494 N	16.4383 E	2005		0.0117
PLONS	CH	47.0492 N	9.3808 E	2002		0.0116
POFI	IV	41.7174 N	13.7120 E	2007		0.0139
POPM	GU	44.0450 N	10.7570 E	2010		0.0083
PP04	7E	51.2548 N	12.6450 E	2006	2006	0.0085
PR01	IV	43.8481 N	12.0606 E	2011	2011	0.0162
PR02	IV	43.8586 N	12.1569 E	2011	2011	0.0115
PR03	7E	51.5962 N	11.9545 E	2006	2008	0.0085
PRI	Y4	44.7164 N	4.5669 E	2004	2006	0.0085
PRK	HL	39.2456 N	26.2650 E	2010		0.0140
PRK	XY	39.2460 N	26.2720 E	2007	2009	0.0140
PSAT	YX	38.3332 N	22.1751 E	2002	2002	0.0151
PSB1	IV	41.2234 N	14.8108 E	2003		0.0112
PST3	IX	40.5609 N	15.2433 E	2009		0.0097
PSZ	GE	47.9184 N	19.8944 E	1995		0.0015
PSZ	HU	47.9182 N	19.8934 E	1995		0.0015
PTCC	IV	46.4075 N	13.3540 E	2003		0.0141
PTL	HL	38.0473 N	23.8638 E	2010		0.0115
PTMD	IV	36.7885 N	11.9934 E	2010	2018	0.0018
PTQR	IV	42.0219 N	13.4006 E	2003		0.0156
PTRJ	IV	41.3641 N	14.5290 E	2007		0.0094
PURA	NI	46.4258 N	12.7419 E	2007		0.0127
PVAQ	PM	37.4037 N	7.7173 W	2006		0.0085
PVO	HP	38.6160 N	21.5250 E	2011		0.0115
PW03	8A	41.6880 N	7.4962 W	2010	2012	0.0018
PW03	X7	43.7754 N	0.5632 W	2012	2013	0.0028
PW05	8A	41.4208 N	6.4807 W	2010	2012	0.0011
PW05	X7	43.6334 N	0.6075 W	2012	2013	0.0033
PW06	8A	40.9958 N	8.2701 W	2011	2012	0.0022
PW06	X7	43.5653 N	0.6613 W	2012	2013	0.0035
PW07	8A	40.9447 N	7.4988 W	2010	2012	0.0018
PW07	X7	43.5090 N	0.7364 W	2012	2013	0.0035
PW08	8A	40.6647 N	6.9899 W	2010	2012	0.0015

PW08	X7	43.4933 N	0.8642 W	2012	2013	0.0032
PW12	8A	40.1971 N	8.8626 W	2010	2011	0.0021
PW12	X7	43.3125 N	1.0373 W	2012	2013	0.0033
PW13	8A	39.7665 N	8.9167 W	2010	2012	0.0019
PW13	X7	43.2265 N	1.1191 W	2012	2013	0.0033
PW14	8A	39.6180 N	8.4106 W	2010	2012	0.0014
PW14	X7	43.1845 N	1.1643 W	2012	2013	0.0034
PW16	8A	39.7682 N	7.0729 W	2010	2012	0.0010
PW16	X7	43.1518 N	1.2559 W	2012	2013	0.0032
PW17	8A	39.3500 N	9.2866 W	2010	2011	0.0023
PW17	X7	43.1086 N	1.2797 W	2012	2013	0.0033
PW18	8A	39.4583 N	7.8858 W	2010	2012	0.0011
PW18	X7	43.0684 N	1.3905 W	2012	2013	0.0048
PW21	X7	42.9481 N	1.5386 W	2012	2013	0.0037
PW27	X7	42.6702 N	1.8539 W	2012	2013	0.0037
PW28	X7	42.6066 N	1.9186 W	2012	2013	0.0036
PW29	X7	42.6014 N	2.0398 W	2012	2013	0.0035
PY05	X7	42.8513 N	0.6161 E	2010	2013	0.0051
PY06	X7	42.7703 N	1.5203 E	2010	2013	0.0038
PY07	X7	42.5602 N	2.4168 E	2011	2012	0.0041
PY43	X7	46.6860 N	1.8690 W	2011	2013	0.0011
PY46	X7	47.7460 N	3.4920 W	2011	2014	0.0012
PYL	HP	36.8955 N	21.7420 E	2007		0.0096
PZUN	BA	40.6458 N	15.8070 E	2008	2018	0.0108
PZUN	IV	40.6458 N	15.8070 E	2018		0.0108
PZZ	GU	44.5068 N	7.1160 E	2007		0.0083
QLNO	IV	44.3242 N	8.3459 E	2003		0.0110
RAFF	IV	37.2225 N	14.3624 E	2005		0.0117
RDP	IV	41.7604 N	12.7103 E	2005		0.0100
REAL	IB	36.4852 N	5.2078 W	2007	2008	0.0030
RESU	IV	37.6468 N	14.0568 E	2008		0.0094
RETH	GR	52.7379 N	9.3610 E	2012		0.0085
RETH	Z3	35.2934 N	24.4948 E	2005	2006	0.0098
REVF	FR	43.7390 N	7.3662 E	2003		0.0095
RIOA	HL	38.2958 N	21.7912 E	2010		0.0124
RISI	SI	46.9480 N	12.0787 E	2006		0.0088
RLS	HL	38.0559 N	21.4648 E	2010		0.0094
RMP	IV	41.8111 N	12.7022 E	2009		0.0113
ROMAN	CH	47.5643 N	9.3360 E	2015		0.0095
RORO	GU	44.1122 N	8.0662 E	2008		0.0149
ROTHE	CH	47.4761 N	7.9209 E	2013		0.0063

ROTM	GU	44.8493 N	8.3527 E	2011		0.0075
RRL	GU	44.9208 N	6.7908 E	2010		0.0066
RSL	FR	45.6882 N	6.6245 E	2010		0.0048
RSM2	IV	43.9377 N	12.4451 E	2012		0.0127
RSP	GU	45.1482 N	7.2653 E	2006		0.0072
RUSF	FR	43.9412 N	5.4837 E	2000		0.0024
SAARA	CH	47.3861 N	8.0438 E	2018		0.0065
SABO	NI	45.9875 N	13.6336 E	2005	2015	0.0133
SABO	OX	45.9875 N	13.6336 E	2016		0.0133
SACR	IV	41.3974 N	14.7057 E	2004		0.0084
SAIG	CH	46.3172 N	6.9666 E	2012		0.0070
SAIRA	CH	47.3027 N	7.0864 E	2011		0.0064
SALAN	CH	46.1442 N	6.9730 E	2001		0.0068
SALB	CH	46.9422 N	8.2745 E	1997	2009	0.0094
SALB	IV	39.8772 N	16.3459 E	2009		0.0094
SALI	IX	40.9300 N	15.1800 E	2009		0.0093
SALO	IV	45.6183 N	10.5243 E	2005		0.0071
SALS	CH	47.2259 N	9.4864 E	1998	2012	0.0094
SALT	CH	46.2173 N	7.3645 E	1992	2005	0.0077
SANT	GE	36.3710 N	25.4590 E	1997	2007	0.0178
SANT	GE	36.3705 N	25.4593 E	2007		0.0178
SANT	HL	36.3705 N	25.4593 E	2010		0.0178
SANT	ZD	36.3710 N	25.4590 E	1996	1997	0.0178
SAOF	FR	43.9860 N	7.5532 E	1995		0.0098
SAPK	CH	47.3305 N	9.4043 E	2015		0.0094
SARC	CH	46.2098 N	7.2564 E	2018		0.0074
SARD	CH	46.7766 N	10.2049 E	2015		0.0079
SARE	CH	47.5149 N	9.4302 E	2014		0.0094
SARG	CH	46.8992 N	8.2510 E	1992	2012	0.0079
SATI	GU	45.8753 N	7.8685 E	2010		0.0063
SAUR	CH	47.5339 N	7.7228 E	2005		0.0058
SAYF	CH	46.2880 N	7.4171 E	1992	2011	0.0079
SAYF2	CH	46.2880 N	7.4170 E	2015		0.0079
SBAE	CH	47.5744 N	7.6107 E	1997	2007	0.0056
SBAF	CH	47.5838 N	7.5920 E	2005		0.0055
SBAH	CH	47.0683 N	9.5084 E	1993	2001	0.0097
SBAJ	CH	47.5669 N	7.5829 E	1998	2009	0.0056
SBAJ2	CH	47.5670 N	7.5824 E	2013		0.0056
SBAK	CH	47.5718 N	7.5928 E	2014		0.0056
SBAM	CH	47.5558 N	7.5916 E	1998	2007	0.0056
SBAM2	CH	47.5557 N	7.5923 E	2014		0.0056

SBAP	CH	47.5724 N	7.5644 E	2005		0.0056
SBAS	CH	47.1938 N	8.5170 E	2014		0.0070
SBAT	CH	47.5586 N	7.5817 E	2005		0.0056
SBAV	CH	47.5633 N	7.6079 E	2013		0.0056
SBAW	CH	47.5476 N	7.6038 E	2013		0.0056
SBEA	CH	47.6984 N	8.5961 E	1992	2012	0.0068
SBET	CH	46.5931 N	9.7612 E	1993	2009	0.0097
SBGN	CH	46.6282 N	9.7484 E	2015		0.0097
SBIF	CH	47.5543 N	7.6285 E	1992	2009	0.0057
SBIK	CH	47.1344 N	7.2470 E	2014		0.0065
SBIS2	CH	47.5411 N	7.5835 E	2008		0.0056
SBRG	CH	46.3110 N	7.9763 E	1992	2017	0.0077
SBRS	CH	46.3169 N	7.9814 E	2012		0.0077
SBUA	CH	47.1590 N	9.4685 E	1992	2009	0.0096
SBUA2	CH	47.1591 N	9.4710 E	2011		0.0096
SBUG	CH	47.1735 N	9.4811 E	1992	2009	0.0096
SBUH	CH	47.1726 N	9.4740 E	2012		0.0096
SBUL	CH	46.6264 N	7.0529 E	2018		0.0069
SBUM	CH	47.1460 N	9.4340 E	1992	2009	0.0096
SBUW	CH	47.1662 N	9.4654 E	1992	1992	0.0096
SCAS	CH	46.1554 N	8.6160 E	1994	2012	0.0067
SCAS2	CH	46.1552 N	8.6148 E	2016		0.0067
SCEL	CH	46.5074 N	9.8554 E	2009		0.0095
SCEM	CH	46.5058 N	9.8411 E	1997	2009	0.0095
SCHAT	CH	46.8315 N	6.8353 E	2017		0.0068
SCHC	CH	47.5325 N	7.6677 E	1992	2012	0.0057
SCHE	CH	47.7117 N	8.6526 E	2001	2009	0.0070
SCHF	SX	50.6772 N	12.4031 E	2002		0.0024
SCHK	CH	46.7889 N	9.5363 E	2015		0.0099
SCHT	CH	47.7116 N	8.6538 E	1992	2001	0.0070
SCOD	CH	46.4705 N	7.1287 E	2016		0.0073
SCOU	CH	46.8540 N	7.1037 E	2008		0.0068
SCTE	IV	40.0724 N	18.4675 E	2006		0.0120
SCUC	CH	46.7980 N	10.3038 E	2005		0.0075
SCUG	CH	46.8561 N	9.5238 E	2011		0.0099
SCUT	CH	46.8597 N	9.5261 E	1992	2008	0.0098
SDAK	CH	46.8005 N	9.8320 E	2015		0.0093
SDAS	CH	46.8020 N	9.8287 E	1992	2003	0.0093
SDES	CH	47.3685 N	7.3399 E	2016		0.0060
SDIF	CH	46.0841 N	7.4018 E	1992	2015	0.0075
SEF1	IV	43.1468 N	12.9476 E	2011		0.0112

SEFS	CH	46.8187 N	8.6485 E	2017		0.0085
SEML	CH	47.6696 N	9.0736 E	1996	2004	0.0088
SEMOS	CH	46.0677 N	6.9350 E	2013		0.0066
SENGL	CH	46.8216 N	8.4105 E	2018		0.0080
SENIN	CH	46.3633 N	7.2994 E	2002		0.0077
SERG	HP	38.4133 N	22.0566 E	2010		0.0169
SERI	HA	37.1609 N	24.4853 E	2010		0.0122
SERI	Z3	37.1610 N	24.4853 E	2005	2007	0.0122
SERI	ZZ	37.1610 N	24.4850 E	2002	2004	0.0122
SERS	IV	39.0359 N	16.6886 E	2005		0.0127
SFEA	CH	46.8458 N	9.4718 E	1992	2017	0.0099
SFEL	CH	47.5326 N	8.2309 E	2016		0.0065
SFI	IV	43.9048 N	11.8470 E	2003		0.0091
SFRA	CH	47.5036 N	7.7091 E	2007		0.0059
SFRS	CH	46.5823 N	7.6563 E	2018		0.0078
SFRU	CH	46.7913 N	7.1579 E	2016		0.0069
SGAG	CH	47.2107 N	9.4493 E	1992	2009	0.0095
SGAK	CH	46.3153 N	7.7414 E	2016		0.0078
SGAS	CH	47.2071 N	9.4706 E	1996	2009	0.0095
SGEM	CH	46.1930 N	6.1300 E	1992	2004	0.0057
SGG	IV	41.3867 N	14.3792 E	2005		0.0093
SGLK	CH	47.0450 N	9.0661 E	2017		0.0092
SGRA	CH	46.1936 N	7.8356 E	2010		0.0074
SGT00	CH	47.4240 N	9.3103 E	2012		0.0094
SGT01	CH	47.4317 N	9.3185 E	2012	2014	0.0124
SGT02	CH	47.5133 N	9.2479 E	2012	2014	0.0089
SGT03	CH	47.3656 N	9.1994 E	2012	2015	0.0093
SGT04	CH	47.3484 N	9.3490 E	2012		0.0132
SGT05	CH	47.4419 N	9.4560 E	2012		0.0124
SGT18	CH	47.4672 N	9.2442 E	2018		0.0094
SGTA	IV	41.1350 N	15.3650 E	2006		0.0097
SHEK	CH	47.4157 N	9.6280 E	2015		0.0092
SHER	CH	46.1853 N	7.3959 E	2017		0.0077
SIEB	CH	46.2954 N	7.5351 E	2012		0.0080
SIES	CH	46.2877 N	7.5485 E	1997	2011	0.0080
SIGR	HT	39.2114 N	25.8553 E	2008		0.0119
SIMPL	CH	46.2396 N	8.0196 E	2009		0.0075
SINS	CH	46.6869 N	7.8641 E	2012		0.0079
SIOE	CH	46.2245 N	7.3842 E	1997	1998	0.0077
SIOP	CH	46.2278 N	7.3483 E	1997	1998	0.0078
SIVA	GE	35.0175 N	24.8100 E	2004	2011	0.0061

SIVA	HL	35.0178 N	24.8120 E	2010		0.0061
SIZS	CH	46.7724 N	9.2053 E	2016		0.0097
SKAF	CH	47.5384 N	7.7199 E	2006		0.0058
SKEH	CH	46.9029 N	8.2715 E	1992	2012	0.0079
SKIA	HA	39.1665 N	23.4661 E	2008		0.0132
SKLW	CH	47.4630 N	8.5674 E	2015		0.0069
SKRK	CH	47.6481 N	9.1806 E	2015		0.0092
SKY	HL	38.8831 N	24.5482 E	2011		0.0134
SKY	XY	38.8831 N	24.5481 E	2007	2009	0.0134
SLAE	CH	46.8996 N	7.2410 E	1992	2016	0.0069
SLCF	CH	47.0830 N	6.7924 E	2016		0.0067
SLCN	IV	40.3900 N	15.6328 E	2003		0.0103
SLE	CH	47.7645 N	8.4924 E	1980		0.0064
SLOP	CH	46.1638 N	8.7906 E	2013		0.0072
SLTM	CH	46.9253 N	9.0003 E	1996	2013	0.0092
SLTM2	CH	46.9236 N	9.0009 E	2011		0.0092
SLUK	CH	47.0479 N	8.3083 E	2014		0.0074
SM0F	CH	46.0021 N	7.3431 E	1992	2005	0.0072
SMAF	CH	46.0567 N	7.9546 E	1992	2014	0.0067
SMAO	CH	46.0989 N	7.0748 E	2012		0.0069
SMAR	CH	46.2079 N	6.9949 E	1992	2017	0.0070
SMAV	CH	46.1002 N	7.0878 E	1992	2008	0.0070
SMELS	CH	47.0465 N	9.4272 E	2018		0.0097
SMFL	CH	47.2100 N	9.5463 E	2014		0.0095
SMG	HL	37.7043 N	26.8377 E	2010		0.0121
SMOE	CH	46.6718 N	6.8011 E	2015		0.0066
SMTH	HL	40.4709 N	25.5304 E	2010		0.0099
SMTK	CH	47.3352 N	9.5896 E	1996	2009	0.0093
SMUK	CH	46.2863 N	6.9406 E	2005		0.0070
SMZA	CH	47.5417 N	7.6583 E	1998	2012	0.0057
SMZW	CH	47.5474 N	7.6471 E	2005		0.0057
SNAL	IV	40.9254 N	15.2091 E	2004		0.0070
SNES	CH	47.0002 N	6.9529 E	1989	2005	0.0068
SNES2	CH	47.0000 N	6.9531 E	2014		0.0068
SNEW	CH	47.1999 N	9.5429 E	1993	2009	0.0095
SNIB	CH	46.1771 N	7.8024 E	2010		0.0074
SNTG	IV	43.2550 N	12.9406 E	2003		0.0101
SNTZ	CH	46.3239 N	7.9883 E	2017		0.0077
SOH	HT	40.8217 N	23.3539 E	2006		0.0085
SOLB	CH	47.2068 N	7.5171 E	2011		0.0064
SPGF	CH	46.6249 N	10.2001 E	1992	2006	0.0082

SRER	CH	47.5116 N	7.5979 E	2011		0.0057
SRFW	CH	47.5532 N	7.8068 E	2017		0.0060
SRHB	CH	47.5713 N	7.6244 E	1996		0.0056
SRHE	CH	47.5856 N	7.6494 E	2013		0.0056
SRHH	CH	47.5798 N	7.6538 E	2013		0.0056
SRNR	CH	47.5110 N	7.6032 E	1997	2007	0.0057
SRS	HT	41.1087 N	23.5950 E	2008		0.0117
SRUG	CH	47.2441 N	9.5258 E	1993	2000	0.0094
SSCN	CH	47.5316 N	7.6697 E	2014		0.0057
SSM1	IV	43.2288 N	13.1770 E	2011		0.0114
SSTS	CH	46.9610 N	8.3568 E	2015		0.0078
SSY	IV	37.1577 N	15.0737 E	2004		0.0142
STAF	CH	46.8052 N	7.2161 E	2008		0.0069
STAM	CH	46.2288 N	7.8625 E	1992	2010	0.0075
STHK	CH	46.7437 N	7.6295 E	2015		0.0076
STIEG	CH	47.4978 N	8.6540 E	2012		0.0073
STRW	CH	47.1165 N	9.5502 E	2014		0.0096
STSP	CH	46.6264 N	10.3332 E	2006		0.0075
STSW	CH	46.3451 N	7.4325 E	1993	2008	0.0080
STSW2	CH	46.3452 N	7.4338 E	2016		0.0080
STV	GU	44.2455 N	7.3260 E	2006		0.0091
SULZ	CH	47.5275 N	8.1115 E	2000		0.0049
SURF	FR	44.4809 N	6.8117 E	2010		0.0111
SUSI	CH	46.0104 N	8.9587 E	2017		0.0073
SVAM	CH	46.6934 N	9.5261 E	1991		0.0099
SVEJ	CH	46.4598 N	6.8394 E	2016		0.0068
SVIL	CH	46.2922 N	7.8865 E	2010		0.0077
SVIO	CH	46.2908 N	7.8803 E	2010		0.0077
SVIP	CH	46.3002 N	7.8636 E	1997	2003	0.0077
SVISP	CH	46.3004 N	7.8775 E	2015		0.0077
SVIT	CH	46.2897 N	7.8850 E	2010		0.0077
SWAS	CH	47.1220 N	9.3088 E	2016		0.0096
SWIK	CH	47.4596 N	9.0346 E	2015		0.0090
SWIS	CH	47.5064 N	8.7300 E	2015		0.0077
SWYZ	CH	47.0238 N	8.6526 E	2018		0.0081
SYVJ	CH	46.7771 N	6.6375 E	2001	2010	0.0064
SZEK	CH	46.0196 N	7.7474 E	2016		0.0068
SZEM	CH	46.6997 N	10.1008 E	1992	2008	0.0085
SZER	CH	46.6975 N	10.0977 E	2006		0.0085
SZUD	CH	47.3693 N	8.5800 E	1992	2005	0.0071
SZUF	CH	47.4662 N	8.5541 E	1998	2009	0.0069

SZWD	CH	46.5528 N	7.3706 E	1993	2017	0.0076
SZWD2	CH	46.5512 N	7.3721 E	2017		0.0076
TIP	MN	39.1794 N	16.7583 E	2003		0.0126
TORNY	CH	46.7736 N	6.9587 E	2000		0.0085
TRIF	IV	43.1148 N	10.9026 E	2010		0.0093
TRIV	IV	41.7666 N	14.5502 E	2005		0.0064
TRTR	IV	42.8081 N	13.9138 E	2005		0.0085
TRULL	CH	47.6487 N	8.6816 E	2003		0.0073
TUE	MN	46.4722 N	9.3473 E	2001		0.0133
VAGA	IV	41.4154 N	14.2342 E	2005		0.0118
VAM	HL	35.4070 N	24.1997 E	2010		0.0081
VANNI	CH	46.2101 N	7.5968 E	2009		0.0093
VDL	CH	46.4832 N	9.4496 E	1983		0.0089
VILL	HA	38.1642 N	23.3122 E	2009		0.0128
VLC	MN	44.1594 N	10.3864 E	2001		0.0133
VLI	HL	36.7180 N	22.9469 E	2010		0.0115
VLX	HP	37.3703 N	22.3793 E	2010		0.0114
VLY	HL	37.8524 N	23.7942 E	2010		0.0075
VULT	IV	40.9549 N	15.6163 E	2005		0.0091
VVLD	IV	41.8696 N	13.6232 E	2003		0.0138
WALHA	CH	47.7528 N	9.1231 E	2013		0.0087
WIMIS	CH	46.6649 N	7.6242 E	2000		0.0101
WOLEN	CH	46.9978 N	7.3688 E	2015		0.0069
XOR	HT	39.3660 N	23.1918 E	2008		0.0117
ZCCA	IV	44.3508 N	10.9765 E	2003		0.0058
ZKR	GE	35.1147 N	26.2170 E	2003	2011	0.0080
ZKR	HL / GE	35.1147 N	26.2169 E	2003		0.0080
ZOVE	IV	45.4536 N	11.4876 E	2011		0.0079
ZUR	CH	47.3692 N	8.5809 E	1998		0.0071